AD_____
(Leave blank)

Award Number:
W81XWH-08-1-0468

TITLE:
Neural Stem Cell Delivery of Therapeutic Antibodies to Treat Breast Cancer Brain Metastases

PRINCIPAL INVESTIGATOR:
Brunhilde Felding-Habermann, PhD

CONTRACTING ORGANIZATION:
The Scripps Research Institute
La Jolla, CA 92037

REPORT DATE:
October 2010

TYPE OF REPORT:
Annual

PREPARED FOR: U.S. Army Medical Research and Materiel Command
Fort Detrick, Maryland 21702-5012

DISTRIBUTION STATEMENT: (Check one)

× Approved for public release; distribution unlimited

REPORT DOCUMENTATION PAGE

Form Approved
OMB No. 0704-0188

1. REPORT DATE *(DD-MM-YYYY)*	**2. REPORT TYPE**	**3. DATES COVERED** *(From - To)*
14-10-2010	Annual	15 SEP 2009 - 14 SEP 2010

4. TITLE AND SUBTITLE
Neural Stem Cell Delivery of Therapeutic Antibodies to Treat Breast Cancer Brain Metastases

5a. CONTRACT NUMBER

5b. GRANT NUMBER
W81XWH-01-1-0468

5c. PROGRAM ELEMENT NUMBER

6. AUTHOR(S)
Brunhilde Felding-Habermann, PhD

Email: brunie@scripps.edu

5d. PROJECT NUMBER

5e. TASK NUMBER

5f. WORK UNIT NUMBER

7. PERFORMING ORGANIZATION NAME(S) AND ADDRESS(ES)
The Scripps Research Institute
10550 North Torrey Pines Road
La Jolla, CA 92037

8. PERFORMING ORGANIZATION REPORT NUMBER

9. SPONSORING / MONITORING AGENCY NAME(S) AND ADDRESS(ES)
U. S. Army Medical Research and
Materiel Command
Fort Derrick, Maryland 21702-5012

10. SPONSOR/MONITOR'S ACRONYM(S)

11. SPONSOR/MONITOR'S REPORT NUMBER(S)

12. DISTRIBUTION / AVAILABILITY STATEMENT
Approved for public release; distribution unlimited,

13. SUPPLEMENTARY NOTES
mechanisms and therapeutic targets for inhibition of breast cancer brain metastasis, establishment of cell and animal models that emulate all steps of clinical breast cancer brain metastasis, development of treatment approaches

14. ABSTRACT
The goal of this study is to develop a new therapeutic approach for clinical inhibition of breast cancer brain metastasis. We have established and validated unique new breast cancer brain metastasis cell models and adapted mouse models to emulate all steps of human breast cancer brain metastasis development and invasive progression. These models are essential new tools for the evaluation of successful new therapies against widespread metastatic brain disease as seen in breast cancer patients. We determined subpopulations of these cells and investigated if cells with a putative stem-like marker profile are responsible for the initiation of brain lesions and successful intracranial metastasis growth. Contrary to current believe, we found that the cells with the putative stem-like marker profile are NOT responsible for highly efficient brain metastatic growth. This finding calls into question approaches that are attempting to target the putative stem cell marker molecules and, if known, their functions. Therefore, our results are valuable for a new outlook guide identification of potential new targets specifically for therapeutic inhibition of brain metastasis in breast cancer. With these advances, and identifying microglial cells as promising host cells for therapeutic use against brain lesions, we have made tangible progress toward new treatment options for breast cancer patients with cerebral metastasis.

15. SUBJECT TERMS
Identification of new targets for therapeutic inhibition of brain metastases; mechanism of action of new targets in brain lesion growth; identification of microglia as a potential therapy delivering host cell type

16. SECURITY CLASSIFICATION OF:			**17. LIMITATION OF ABSTRACT**	**18. NUMBER OF PAGES**	**19a. NAME OF RESPONSIBLE PERSON**
a. REPORT	**b. ABSTRACT**	**c. THIS PAGE**			USAMRMC
U	U	U	UU	42	**19b. TELEPHONE NUMBER** *(include area code)*

Table of Contents

Grant: W81X WH-01-1-0468
Title: **Delivery of Therapeutic Antibodies to Treat Breast Cancer Brain Metastases**

Report: Sept 2009 – Sept 2010

Introduction

Brain metastases are among the most feared complications in breast cancer (1-3). Today, nearly 30% of patients with advanced breast cancer are eventually diagnosed with brain lesions, making breast tumors the main source of metastatic brain disease in women (4, 5). However, treatment options are limited and in most cases prolong patient survival only for a few weeks or months, often associated with severe side effects. Current treatment options are surgery, if isolated brain lesions can be safely removed, gamma knife surgery and whole brain radiation. Unfortunately, cases with operable lesions are rare and brain metastatic disease is most often widespread and ultimately fails to respond to these therapies. Therefore, it is imperative to develop new, effective regimens that prevent and control this stage of the disease. Thus, the goal of our project is to develop mechanisms through which therapeutic antibodies can be successfully delivered to breast cancer brain lesions to effectively interfere with intracranial tumor cell growth and expansion. Today's clinical regimen of antibodies against metastatic breast cancer progression include Herceptin, a human antibody directed against the Her2 receptor expressed on an aggressive subgroup of breast cancer types that frequently metastasizes to all major target organs of breast cancer metastasis, including the brain. Herceptin treatment has been successfully used in the clinic and a high percentage of treated patients, at least initially, respond well to this therapy with regression of extracranial metastatic burden. However, the incidence of brain lesions in these patients is rising (6). Failure of the therapeutic antibody to reach breast cancer cells has been held responsible for progression of brain metastasis in the central nervous system under the antibody treatment (7-10).

As antibodies could potentially serve as effective anti-cancer agents against brain metastases, a major hurdle to overcome in treatment of breast cancer brain metastases is to develop delivery systems that will allow antibody molecules, or their effective fragments, to pass the blood brain barrier and reach widespread lesions within the central nervous system.

Body

The aims of our study are:

1. To develop components for a functional and clinically relevant model of breast cancer brain metastasis and neural progenitor cell scFv therapy
2. To generate a pre-clinical model of neural progenitor-scFv therapy and test its efficacy in vivo

During the past funding period, we have made major progress toward these aims and reached several of our milestones defined in the statement of work. Guided by our results, we have also expanded the questions addressed, to optimize the outcome toward better understanding of breast cancer brain lesions development and finding of effective ways to treat lesions in the central nervous system.

Milestones reached:

Clinically relevant model of breast cancer brain metastasis

- We analyzed initial steps of brain colonization by circulating breast cancer cells from the blood stream and investigated the timing and mechanism involved in tumor cell penetration of the blood brain barrier

- In analyzing early steps of breast cancer brain metastasis, namely the initial colonization of the brain by circulating breast cancer cells and their invasion of the brain tissue, we identified early as well as persisting host cell reactions to the arrival of breast cancer cells in the brain. We have progressed to investigating mechanisms through which these host cells, namely astrocytes and microglial cells, interact with brain metastatic breast cancer cells and influence the development of breast cancer brain lesions.

- We have developed two new unique cell models of human breast cancer brain metastasis. These cell models were derived from surgical specimens of patients with brain metastatic disease. These models and their characteristics will be major contributions to the field of breast cancer brain metastasis as there are currently no suitable models that accurately emulate the human situation and are amenable to experimentation in vitro and in vivo (mouse model).

- We have identified cell subpopulations within these new brain metastatic cell models that have distinct intracranial growth properties.

- Investigation of currently believed stem cell markers expressed in these subpopulations revealed that putative stem cell markers do NOT identify the most aggressively growing cell population and do not represent the cell population that is capable most effectively initiating brain metastatic growth.

- Functional and gene expression analyses of the stem cell marker expressing and non-stem cell marker expressing subpopulations is beginning to reveal new mechanisms involved in the control of breast cancer brain metastatic growth. The results are also beginning to identify new potential targets for therapeutic inhibition.

As brain metastases are difficult to treat and mostly develop late during progressive metastatic disease, breast cancer patients at risk would benefit from the development of prevention as well as improved treatments. This requires knowledge of the initial events that lead to brain metastasis. Our study revealed cellular events during the initiation of brain metastasis by breast cancer cells and documents the earliest host responses to incoming cancer cells after carotid artery injection in immune deficient and immune competent mouse models. Our findings capture and characterize heterogeneous astrocytic and microglial reactions to the arrest and extravasation of cancer cells in the brain, showing immediate and drastic changes in the brain microenvironment upon arrival of individual cancer cells. We identified reactive astrocytes as the most active host cell population that immediately localizes to individual invading tumor cells and continuously associates with growing metastatic lesions. Up-regulation of MMP-9 associated with astrocyte activation in the immediate vicinity of extravasating cancer cells might support their progression. Early involvement of different host cell types indicates environmental clues that might co-determine whether a single cancer cell progresses to macrometastasis or remains dormant. Thus, information on the initial interplay between brain homing tumor cells and reactive host cells may help develop strategies for prevention and treatment of symptomatic breast cancer brain metastases.

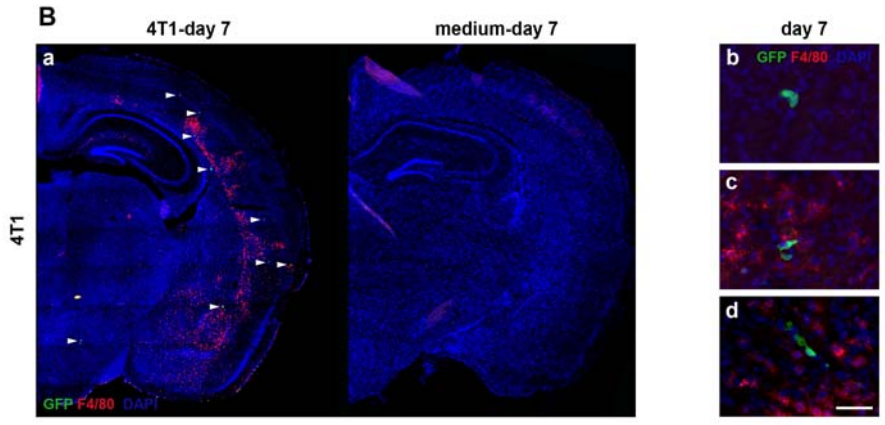

Figure 1. Microglial cell responses to invading cancer cells are heterogeneous. Microglial activation in response to cancer cell invasion varies at early as well as late stages, as detected by immunofluorescence analysis. **(A)** MDA-MB-435 cells in immunosuppressed mice; **a:** Diverse microglial responses (green) to incoming cancer cells (red) on day 7. Responses include **b:** absence of microglial cells, **c:** presence of hypertrophic stellate activated, or **d:** amoeboid reactive microglial cells. Similarly, on day 50, **e:** some macrometastases show no microglial involvement, or **f:** contain stellate or **g:** amoeboid microglia. Bars: 100 µm (a), 50 µm (b-g).

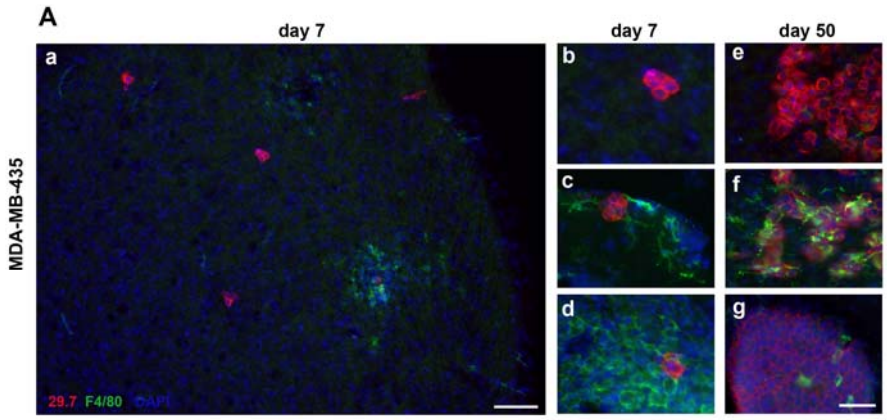

Figure 1. Microglial cell responses to invading cancer cells are heterogeneous (continued)

(B) 4T1 cells in immunocompetent mice; **a:** Distribution of activated microglia (red) in the mouse brain 7 days after carotid artery injection of cancer cells (left) or medium alone (right). White arrowheads mark the GFP-labeled cancer cells (green). Diverse microglial responses to cancer cells include **b:** absence of microglial cells, **c:** presence of hypertrophic stellate, or **d:** reactive amoeboid microglial cells. Bar: 50 µm.

To understand the nature of brain metastatic breast cancer cells and identify key functional parameters of their brain metastatic activity as therapeutic targets, we established two new cell models that were derived from actual surgical specimens of brain lesions from breast cancer patients. Figure 2 shows RJBr1, one of our new brain metastatic cell models grown in culture and as xenografts in the central nervous system of immuno deficient SCID mice. These tumor cells are ER-/PR+ and Her2+ and show aggressive rapid intracranial growth and invasive expansion within the central nervous system when implanted into the brain microenvironment.

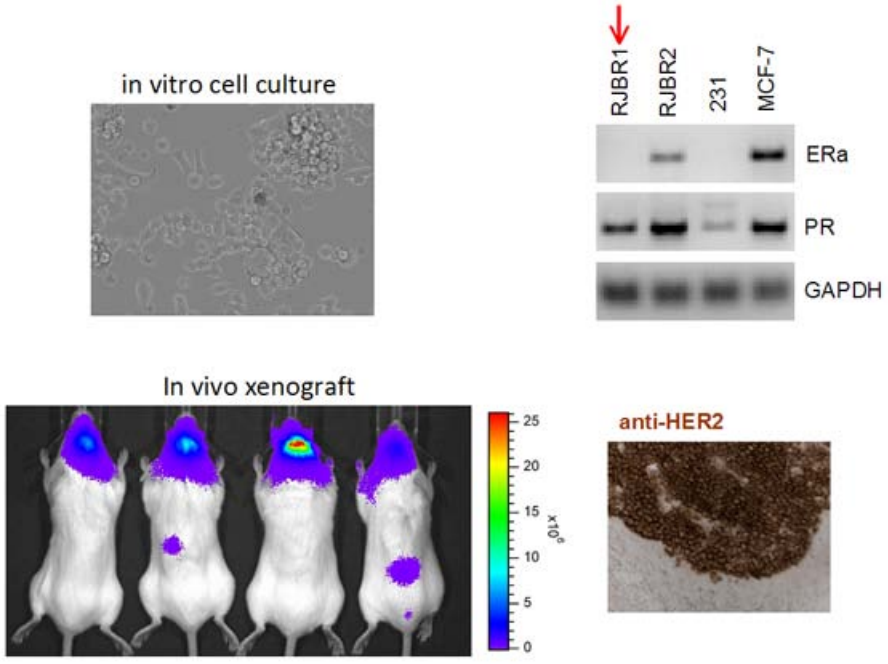

Figure 2. RJBR1, a new cell model of breast cancer brain metastasis. In culture, these cells grow with an epithelial like morphology. Once implanted into the brain of female SCID mice, the cells rapidly expand and invasively infiltrate the central nervous system. By gene expression, RJBr1 cells are ER- and Her2+. Her2 protein expression was confirmed by in situ immunohisto chemistry.

To address the question of whether a particular subpopulation of cells within the parental cells are responsible for brain metastatic growth and therefore specifically suited for therapeutic targeting, we isolated subpopulations of RJBr1 cells from brain metastatic lesions grown in the mouse model. Current concepts hold cancer cells with a stem-like phenotype responsible for tumor and metastasis initiating capabilities (11). One of the currently used 'markers' is expression of adhehyde dehydrogenase 1, ALDH1, to identify a cancer cell subpopulation with a stem-like phenotype (12). This was especially shown for cancers of the breast, lung, colon, and prostate (13-16). We therefore analyzed ALDH expression in RJBr1 cells based on the Aldefluor assay (17). Figure 3 shows that RJBr1 cells from brain metastatic lesions grown in the mouse brain contain an

Aldefluor positive and a negative subpopulation. This was confirmed by immunohhistochemistry in brain metastatic lesions. After sorting the cells apart by flow cytometry and based on Aldefluor activity, two distinct cell subpolations were confirmed based on ALDH1 gene expression. To assess whether the ALDH1 positive subpopulation was associated with expression of markers currently assigned to a stem-like breast cancer cell population, we analyzed CD133 expression in both ALDH1 positive and negative subpopulations (18). As shown in Figure 4, CD133 segregates with ALDH1 expression, indicating that the ALDH1 positive cells indeed express additional markers of stemness.

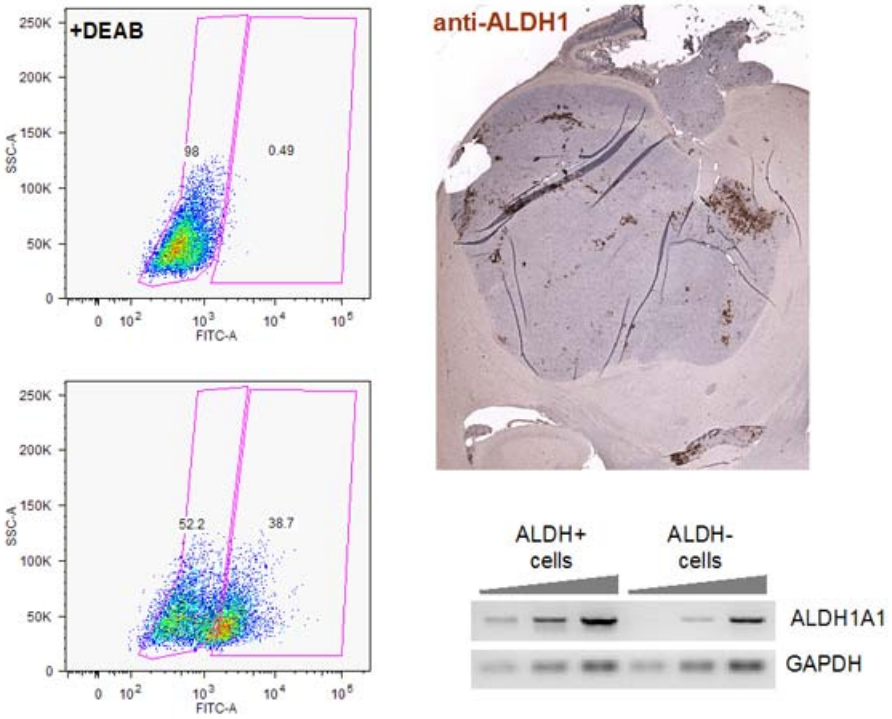

Figure 3. Brain metastatic lesions from RJBr1 implants contain ALDH positive and negative subpopulations.
Left: Brain lesion derived human breast cancer cells were analyzed by the Aldefluor assay and flow cytometry, showing Aldefluor positive and negative cells. Addition of DEAB, an inhibitor of adehyde dehydrogenase activity, identifies the region in which the ALDH negative population can be identified. *Right top:* immunohistochemisty analysis of brain metastatic lesion growth in the SCID mouse brain. H&E staining. The lesion appears light blue, and ALDH1 positive cells within the lesion are identified by specific antibody staining (brown). *Right bottom:* ALDH1A1 gene expression by in the ALDH1 positive and ALDH1 negative subpopulations sorted from the brain lesions.

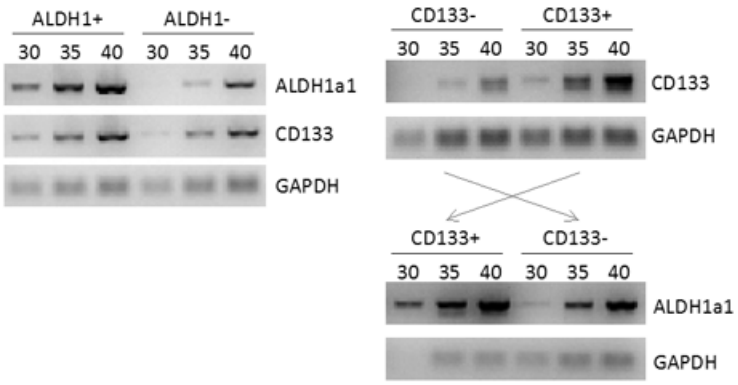

Figure 4. Stem-like marker expression in ALDH1 positive and ALDH1 negative subpopulations of RJBr1 brain metastatic lesions.
CD133 was used as a putative marker whose expression has been associated with a stem like cancer cells subpopulation. Expression of ALDH1 positive and ALDH1 negative populations from RJBr1 brain lesions after flow cytometry sorting based on the Aldefluor assay. ALDH1 and CD133 gene expression by PCR (number of cycles indidated above each lane).

Having identified breast cancer cell subpopulation in xenograft brain metastatic lesions of RJBr1 cells, we next asked if the subpopulation with the stem cell marker phenotype was primarily responsible for intracranial growth. To address this question, ALDH1+ cells versus ALDH- cells were implanted into the SCID mouse brain at different cell numbers, and brain metastatic growth was monitored by non-invasive bioluminescence imaging. Figure 5 shows that, surprisingly, the ALDH1 negative breast cancer cell subpopulation grew much more efficiently and faster than the ALDH positive subpopulation. This was confirmed by analyzing the histology of the affected mouse brains (Figure 6). This analysis also showed that in most experimental mice,

the ALDH1 positive cell population actually perished and never formed an implant lesion. This finding was confirmed by quantifying a proliferation dependent antigen (Ki67) whose expression indicates the presence of cells actively moving through the cell cycle (Figure 7).

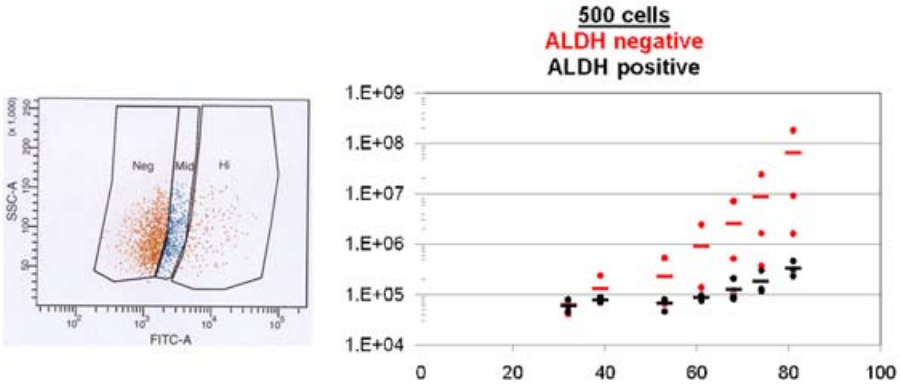

Figure 5. Brain metastatic growth of ALDH positive and ALDH negative subpopulations.
Left: RJBR1 cells from brain metastatic lesions were sorted by flow cytometry for ALDH positive (yellow) versus negative populations (orange) (blue intermediate population was not used). *Right:* Then, 500 cells of each population per mouse were implanted into the brains of SCID mice and lesion growth followed by non-invasive bioluminescence imaging over time (x-axis in the graph denotes days after implant, y-axis denotes intracranial growth signal by the tumor cells in

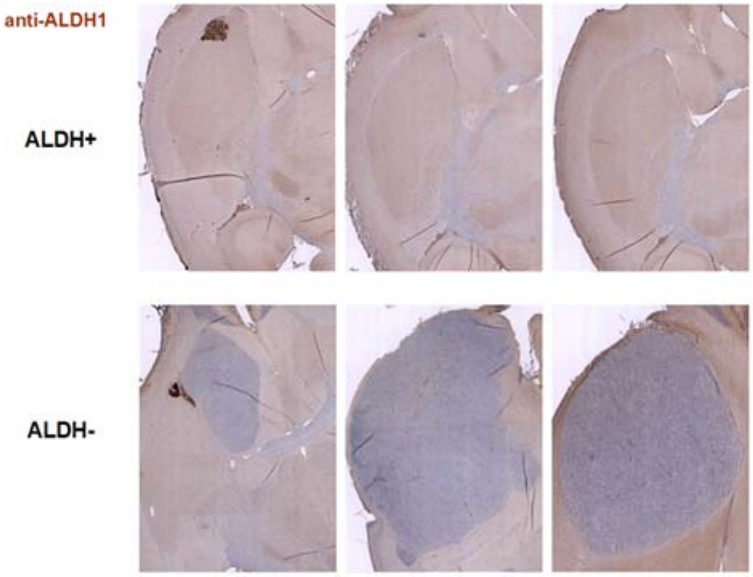

Figure 6. Intracranial growth of ALDH + versus ALDH$^-$ RJBR1 cells in the SCID mouse brain.
Histological analysis of brain lesions 60 days after implanting 500 tumor cells of each subpopulation. Each image represents one mouse brain. *Top:* Most brains showed no lesion growth, the brain on the left shows a small ALDH1 positive lesion at the implant site, indicating survival of some of the tumor cells. *Bottom:* Large lesions 60 days after implanting ALDH negative cells from. The brain in the left panel indicates a small portion of ALDH1 positive cells.

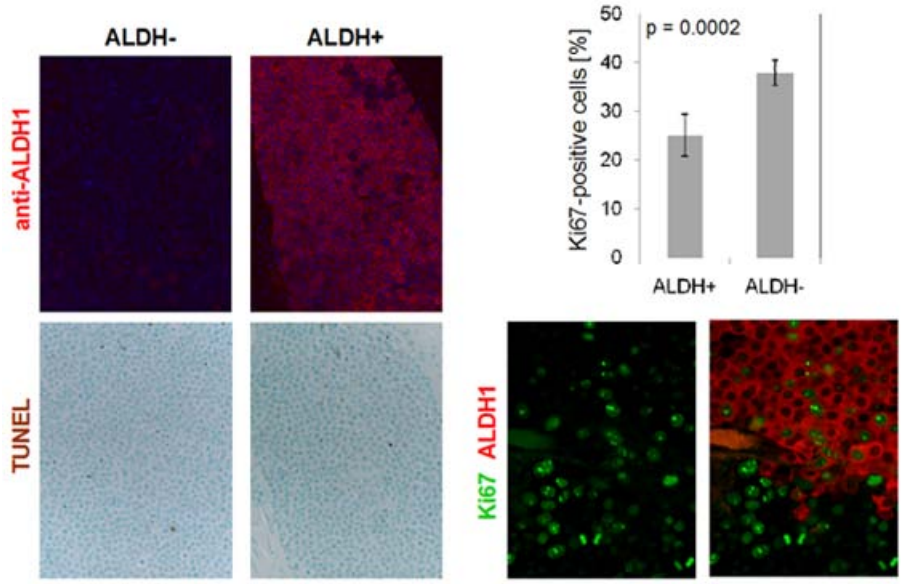

Figure 7. ALDH1 positive versus negative expression is maintained in advanced brain metastatic lesions, and ALDH1 negativity is associated with enhanced breast cancer cell proliferation in the brain.
Brain metastatic lesions were analyzed 60 days after implanting 500 ALDH1 positive versus negative RJBR1 cells into the SCID mouse brain. Tunel staining revealed that both lesion types do not contain appreciable numbers of apoptotic cells. Ki67 staining revealed that ALDH1 negative lesions clearly contain more cells actively undergoing cell cycle progression.

Our findings indicate that breast cancer brain metastatic growth does not depend on the presence of cells that display markers associated with a cancer stem like phenotype. In fact, the breast cancer cell subpopulation expressing stem like markers was explicitly unable to form intracranial lesions, whereas the stem marker negative cells were responsible for lesion formation. This is an unexpected finding and goes against current dogma that a stem-like subpopulation of breast cancer cells are the metastasis initiating cells (13).

Ongoing and future activities based on these findings:

Importantly, our identification of distinct brain metastatic cell subpopulations, expressing either a brain lesion promoting or a non-promoting phenotype in the mouse model, allows us to compare these cells based on their gene expression profiles and functional behavior. We have performed gene expression array analyses and the results will be used to interrogate the presence of functional treats that may be responsible for breast cancer brain metastatic growth. Importantly, findings from these analyses will also allow us to define new functional targets for therapeutic inhibition of breast cancer brain metastasis.

Combining this knowledge with our new information that microglial cells might be potential executors of therapeutic strategies, either on their own account or after specific harnessing, provides unique new information for downstream development of improved therapeutic approaches against breast cancer brain metastasis. Even though a distinct reactivity of astrocytes to incoming and expanding brain metastatic breast cancer cells was appreciated as well, microglial cells are of particular interest in the context of identifying putative therapy carrier host cell types. The main reason for this is that microglial cells originate in the bone marrow and might be accessible in the clinic for preparing or harnessing of therapeutic host cells for each individual patient.

A second set of investigations was dedicated to a functional target that we had previously identified and functionally validated: the activated conformer of breast cancer cell integrin $\alpha v\beta 3$ expressed by brain metastatic cells.

Validation of activated integrin $\alpha v\beta 3$ as a promising target for scFv therapy

In preparation for the demanding task of developing a neural progenitor delivered scFv therapy against breast cancer brain metastases, we have established clinically relevant therapeutic activity of the scFv antibodies directed against the high affinity form of integrin $\alpha v\beta 3$. The results from this part of the study have now been published.

Targeting activated integrin $\alpha v\beta 3$ with patient-derived antibodies impacts late-stage multiorgan Metastasis

Staflin K, Krueger JS, Hachmann J, Forsyth JS, Lorger M, Steiniger SC, Pop C, Salvesen G, Janda KD, Felding-Habermann B
2010 Clinical and Experimental Metastasis 27(4): 217-231

Advanced metastatic disease is difficult to manage and specific therapeutic targets are rare. We showed earlier that metastatic breast cancer cells use the activated conformer of adhesion receptor integrin $\alpha v\beta 3$ for dissemination. We now investigated if targeting this form of the receptor can impact advanced metastatic disease, and we analyzed the mechanisms involved. Treatment of advanced multi-organ metastasis in SCID mice with patient-derived scFv antibodies specific for activated integrin $\alpha v\beta 3$ caused stagnation and regression of metastatic growth. The antibodies specifically localized to tumor lesions *in vivo* and inhibited $\alpha v\beta 3$ ligand binding at nanomolar levels *in vitro*. At the cellular level, the scFs associated rapidly with high affinity $\alpha v\beta 3$ and dissociated extremely slowly. Thus, the scFvs occupy the receptor on metastatic tumor cells for prolonged periods of time, allowing for inhibition of established cell interaction with natural $\alpha v\beta 3$ ligands. Potential

apoptosis inducing effects of the antibodies through interaction with caspase-3 were studied as potential additional mechanism of treatment response. However, in contrast to a previous concept, neither the RGD-containing ligand mimetic scFvs nor RGD peptides bound or activated caspase-3 at the cellular or molecular level. This indicates that the treatment effects seen in the animal model are primarily due to antibody interference with $\alpha v\beta 3$ ligation. Inhibition of advanced metastatic disease by treatment with cancer patient derived single chain antibodies against the activated conformer of integrin $\alpha v\beta 3$ identifies this form of the receptor as a suitable target for therapy.

Key Research Accomplishments

- We developed new models of human breast cancer brain metastasis and animal models that emulate all stages of brain metastasis in breast cancer
- We investigated the characteristics and marker expression of subpopulations of these truly brain metastasis derived breast cancer cells. Our results indicate that currently used putative markers for stem-like breast cancer cells are NOT associated with the cell population that exhibits the most aggressive brain metastatic growth.
- Gene array profiling analysis of the stem-like (poorly growing) subpopulation versus the non-stem-like (fast and efficiently growing) subpopulation will reveal a basis for the understanding of growth regulation within the brain microenvironment, and possibly identify new functional targets for therapeutic inhibition.
- We identified initial and persisting host cell responses to invading breast cancer cells within the brain tissue
- Among the earliest and persisting host cell responses are microglial localization and activation in the immediate vicinity of incoming and expanding breast cancer brain metastatic cells
- With these findings, we identified microglial cells and potentially their precursor cells as possible alternative host cells to neural stem cells for delivery of therapeutic molecules to early as well as widespread breast cancer brain metastases.
- As microglial precursors originate in the bone marrow and, as we document, actively seek out even individual brain metastatic breast cancer cells, these microglial cells can be superior host cells for inhibition of breast cancer brain metastasis, as neural stem cells are difficult to access and potentially manipulate for therapeutic use.

Reportable Outcomes

List of publications with DOD grant W81XWH-01-1-0468

Lorger M, Felding-Habermann B (2010) Capturing changes in the brain microenvironment during initial steps of brain metastasis. Am J Pathol 176 (6): 2958-2971

Staflin K, Krueger JS, Hachmann J, Forsyth JS, Lorger M, Steininger SC, Pop C, Salvesen G, Janda KD, Felding-Habermann B (2010) Targeting activated integrin $\alpha v\beta 3$ with patient-derived antibodies impacts late-

state multiorgan metastasis. Clinical and Experimental Metastasis 27 (4):217-231

Symposium Abstracts and Lectures associated with DOD grant W81XWH-01-1-0468

Lorger M. and Felding-Habermann B. (2010) Interactions between breast cancer brain metastasis and their microenvironment. *Joint Metastasis Research Society-AACR Conference: Metastasis and the Tumor Microenvironment, Philadelphia, PA, September 12-15 2010*

Staflin K, F ogal V, Fer nandez-Santidrian A, R uoslahti E, Felding-Habermann B (2010) The r ole of p32 in breast cancer brain metastasis. *AACR 2010 Annual Conference, Washington DC 17-21 April 2010*

Invited oral presentations given by B. Felding-Habermann associated with DOD grant W81XWH-01-1-0468

Lurie Comprehensive Cancer Center, Northwestern University, Chicago, Feb 25-26, 2010
Mechanisms and inhibition of breast cancer brain metastasis

California Breast Cancer Symposium, Oakland, Sept 24-25, 2010
New Approaches for Targeting Breast Cancer Brain Metastases

Disclosures associated with DOD grant W81XWH-01-1-0468

Felding-Habermann B, O'Sullivan D, Lorger M 2010 "Novel Cell Models of Breast Cancer Brain Metastasis" (Disclosure)

List of community presentations by B. Felding-Habermann with DOD grant W81XWH-01-1-0468

2010 "Targeting Breast Cancer Brain Metastasis" Presentation at the Breast Cancer Golf Tournament for the Cure. Lomas Santa Fe Country Club (Solana Beach, CA)

2010 Teaching activity for Project LEAD, the National Breast Cancer Coalition's premier science training program for activists, that has created a revolution in the world of breast cancer research and public policy (La Jolla, CA)

Conclusion

The goal of this study is to develop a new therapeutic approach for clinical inhibition of breast cancer brain metastasis. Our work to date has identified a new molecular target for treatment of metastatic brain disease in breast cancer patients and provided antibody tools that successfully interrupt breast cancer metastasis in a mouse model. Systemic application of the antibodies does not sufficiently reach brain lesions to interfere with their development and progression. Delivery strategies are being developed to bring therapeutic antibodies or their fragments to brain metastatic lesions and inhibit their proliferation.

We have established and validated unique new breast cancer brain metastasis cell models and adapted mouse models to emulate all steps of human breast cancer brain metastasis development and invasive progression. These models are essential new tools for the evaluation of successful new therapies against widespread metastatic brain disease as seen in breast cancer patients. During the last funding period, we have thoroughly investigated one of the new brain metastatic breast cancer cell models. We have determined subpopulations of these cells and investigated if cells with a putative stem-like marker profile are responsible

for the initiation of brain lesions and successful intracranial metastasis growth. Contrary to current believe, we found that the cells with the putative stem-like marker profile are NOT responsible for highly efficient brain metastatic growth. This finding calls into question approaches that are attempting to target the putative stem cell marker molecules and, if known, their functions. Therefore, our results are valuable for a new outlook regarding guidance to identify potential new targets specifically for therapeutic inhibition of brain metastasis in breast cancer.

By investigating the earliest as well as later steps of breast cancer brain metastasis, and by specifically analyzing host cell types that react to the arrival and expansion of the tumor cells within the brain microenvironment, we identified a new promising host cell type that might be amenable to carrying therapeutic regimens to developing brain metastases. These cells are the microglial cells of the brain. The microglial cells are potential new host cell types for therapy delivery as they originate outside the brain in the bone marrow. Once the microglial precursor cells enter the brain from the blood stream, they specialize within the brain microenvironment and assume macrophage like functions. This finding is highly relevant and could have broad clinical significance. Microglial precursor cells could be superior to neural stem cells as potential therapeutic host cell types for two major reasons: even though neural stem cells are highly efficient in seeking even widespread metastatic cells within the brain and central nervous system, we had difficulties to efficiently express therapeutic antibody fragments in these cells. Microglial cells can be a superior alternative. The precursors of microglial cells, originate in the bone marrow and are therefore more easily accessible than neural stem cells. For optimum compatibility, microglial precursors could be isolated from each individual patient and used for efficient targeting of each individual patient's own tumor burden in the brain.

With these advances, we have made tangible progress toward new treatment options for breast cancer patients with cerebral metastasis.

References

(1) Kirsch DG, Loeffler JS. Brain metastases in patients with breast cancer: new horizons. Clin Breast Cancer 2005;6:115-24.

(2) Weil RJ, Palmieri DC, Bronder JL, Stark AM, Steeg PS. Breast cancer metastasis to the central nervous system. Am J Pathol 2005;167:913-20.

(3) Palmieri D, Chambers AF, Felding-Habermann B, Huang S, Steeg PS. The biology of metastasis to a sanctuary site. Clin Cancer Res 2007;13:1656-62.

(4) Clayton AJ, Danson S, Jolly S, Ryder WD, Burt PA, Stewart AL, et al. Incidence of cerebral metastases in patients treated with trastuzumab for metastatic breast cancer. Br J Cancer 2004;91:639-43.

(5) Yates JR, III, Eng JK, McCormack AL, Schieltz D. Method to correlate tandem mass spectra of modified peptides to amino acid sequences in the protein database. Anal Chem 1995;67:1426-36.

(6) Piccart-Gebhart MJ, Procter M, Leyland-Jones B, Goldhirsch A, Untch M, Smith I, et al. Trastuzumab after adjuvant chemotherapy in HER2-positive breast cancer. N Engl J Med 2005;353:1659-72.

(7) Peacock KH, Lesser GJ. Current therapeutic approaches in patients with brain metastases. Curr Treat Options Oncol 2006;7:479-89.

(8) Nieder C, Grosu AL, Astner S, Thamm R, Molls M. Integration of chemotherapy into current treatment strategies for brain metastases from solid tumors. Radiat Oncol 2006;1:19.:19.

(9) Lin NU, Bellon JR, Winer EP. CNS metastases in breast cancer. J Clin Oncol 2004;22:3608-17.

(10) Klos KJ, O'Neill BP. Brain metastases. Neurologist 2004;10:31-46.

(11) Blick T, Hugo H, Widodo E, Waltham M, Pinto C, Mani SA, et al. Epithelial mesenchymal transition traits in human breast cancer cell lines parallel the CD44(hi/)CD24 (lo/-) stem cell phenotype in human breast cancer. J Mammary Gland Biol Neoplasia 2010;15:235-52.

(12) Ginestier C, Hur MH, Charafe-Jauffret E, Monville F, Dutcher J, Brown M, et al. ALDH1 is a marker of normal and malignant human mammary stem cells and a predictor of poor clinical outcome. Cell Stem Cell 2007;1:555-67.

(13) Charafe-Jauffret E, Ginestier C, Iovino F, Wicinski J, Cervera N, Finetti P, et al. Breast cancer cell lines contain functional cancer stem cells with metastatic capacity and a distinct molecular signature. Cancer Res 2009;69:1302-13.

(14) Huang EH, Hynes MJ, Zhang T, Ginestier C, Dontu G, Appelman H, et al. Aldehyde dehydrogenase 1 is a marker for normal and malignant human colonic stem cells (SC) and tracks SC overpopulation during colon tumorigenesis. Cancer Res 2009;69:3382-9.

(15) Jiang F, Qiu Q, Khanna A, Todd NW, Deepak J, Xing L, et al. Aldehyde dehydrogenase 1 is a tumor stem cell-associated marker in lung cancer. Mol Cancer Res 2009;7:330-8.

(16) Levi BP, Yilmaz OH, Duester G, Morrison SJ. Aldehyde dehydrogenase 1a1 is dispensable for stem cell function in the mouse hematopoietic and nervous systems. Blood 2009;113:1670-80.

(17) Alison MR, Guppy NJ, Lim SM, Nicholson LJ. Finding cancer stem cells: are aldehyde dehydrogenases fit for purpose? J Pathol 2010.

(18) Shipitsin M, Campbell LL, Argani P, Weremowicz S, Bloushtain-Qimron N, Yao J, et al. Molecular definition of breast tumor heterogeneity. Cancer Cell 2007;11:259-73.

Appendices

Publications

Lorger M, Felding-Habermann B Capturing changes in the brain microenvironment during initial steps of brain metastasis (2010) Am J Pathol 176 (6): 2958-2971

Staflin K, Krueger JS, Hachmann J, Forsyth JS, Lorger M, Steininger SC, Pop C, Salvesen G, Janda KD, Felding-Habermann B Targeting activated integrin $\alpha v\beta 3$ with patient-derived antibodies impacts late-state multiorgan metastasis (2010) Clin Exp Metastasis 27 (4):217-231

The American Journal of Pathology, Vol. 176, No. 6, June 2010

DOI: 10.2353/ajpath.2010.090838

Tumorigenesis and Neoplastic Progression

Capturing Changes in the Brain Microenvironment during Initial Steps of Breast Cancer Brain Metastasis

Mihaela Lorger and Brunhilde Felding-Habermann

From the Department of Molecular and Experimental Medicine, The Scripps Research Institute, La Jolla, California

Brain metastases are difficult to treat and mostly develop late during progressive metastatic disease. Patients at risk would benefit from the development of prevention and improved treatments. This requires knowledge of the initial events that lead to brain metastasis. The present study reveals cellular events during the initiation of brain metastasis by breast cancer cells and documents the earliest host responses to incoming cancer cells after carotid artery injection in immunodeficient and immunocompetent mouse models. Our findings capture and characterize heterogeneous astrocytic and microglial reactions to the arrest and extravasation of cancer cells in the brain, showing immediate and drastic changes in the brain microenvironment on arrival of individual cancer cells. We identified reactive astrocytes as the most active host cell population that immediately localizes to individual invading tumor cells and continuously associates with growing metastatic lesions. Upregulation of matrix metalloproteinase-9 associated with astrocyte activation in the immediate vicinity of extravasating cancer cells might support their progression. Early involvement of different host cell types indicates environmental clues that might codetermine whether a single cancer cell progresses to macrometastasis or remains dormant. Thus, information on the initial interplay between brain homing tumor cells and reactive host cells may help develop strategies for prevention and treatment of symptomatic breast cancer brain metastases. ***(Am J Pathol 2010, 176:000–000; DOI: 10.2353/ajpath.2010.090838)***

Brain metastases are diagnosed in 10 to 40% of all cancer patients, and the incidence is rising as patients live longer due to improved treatments for extracranial metastases.[1,2] Brain lesions are most frequently associated with lung cancer, breast cancer, and melanoma.[1,2] Unfortunately, brain metastases are still very difficult to treat and the mechanisms underlying their establishment and progression are poorly understood. Thus, information in this direction and models for analysis are a prerequisite for the development of new, efficient therapies.

The essential role of the tumor microenvironment in cancer progression has been well documented for extracranial malignancies, and recent findings indicate that the tumor microenvironment might be a suitable target in anticancer therapies, as well as a valuable biomarker for prognostic purposes.[3–5] The brain provides a unique environment with paracrine growth factors that differ from most other organs.[6,7] The involvement of brain-resident cells including brain endothelial cells, microglia, and astrocytes in the pathology of primary and metastatic brain tumors is only partially understood. Brain endothelial cells are the first host cell type that circulating cancer cells encounter when they arrest within the brain microvasculature. In addition to posing the initial barrier for brain invasion, endothelial cells and their basement membrane seem to play important roles in supporting the growth of brain metastases as well as brain tumor stem cells.[8–10] So far, only a few studies documented cancer cell arrest and extravasation in the brain *in vivo*[11–13]. Once incoming cancer cells begin to infiltrate the brain tissue, they encounter a number of host cell types that may respond to their arrival. Microglia constitute the tissue macrophages of the central nervous system and are the main respond-

Supported by postdoctoral fellowship from the Susan G. Komen Breast Cancer Foundation (PDF0707935; to M.L.), National Institutes of Health grants CA095458 and CA112287 (to B.F.-H.), California Breast Cancer Research Program grants 12NB0176 and 13NB0180 (to B.F.-H.), and Department of Defense grant W81XWH-08-1-0468 (to B.F.-H.).

Accepted for publication January 26, 2010.

Supplemental material for this article can be found on *http://ajp.amjpathol.org*.

Address reprint requests to Brunhilde Felding-Habermann, Ph.D., and Mihaela Lorger, Ph.D., Department of Molecular and Experimental Medicine, The Scripps Research Institute, 10550 North Torrey Pines Road, MEM-150, La Jolla, CA 92037. E-mail: brunie@scripps.edu or mlorger@scripps.edu.

ers to primary brain tumors. Activated microglia can be frequently found in the vicinity of brain lesions,[14–18] and the inhibition of microglial activation has been shown to significantly reduce glioma proliferation.[14] Microglia secrete multiple cytokines, growth factors, and enzymes that can directly or indirectly lead to immunosuppression, angiogenesis, tumor proliferation, and invasion.[15,17,19,20] In contrast to these cancer promoting effects, however, microglia has also been reported to elicit cytotoxicity toward lung cancer brain metastases.[21] Thus, microglial cells seem to play diverse roles in cancer progression, which might be related to their heterogeneity and distinct stages of activation. In addition to microglia, reactive astrocytes have been frequently observed in the vicinity of primary and metastatic brain tumors in animal models as well as in human patients.[6,15,22] Astrocytes were shown to support brain tumor growth by secretion of cytokines, heparanase, and neurotrophic factors such as transforming growth factor-α, Stromal cell-derived factor 1 (SDF-1) Sphingosin-1 phosphate, and Glial cell line-derived neurotrophic factor.[17,23–25] Furthermore, an immortalized astrocyte cell line has been recently shown to promote cell division and survival in lung adenocarcinoma cells *in vitro*.[26]

Although the microenvironment of established brain tumors has been intensively studied, the induction of changes in the brain during the initial steps of cancer cell invasion from the bloodstream has not been described previously. This is probably due to challenges in the establishment of specialized animal models and techniques that allow efficient and detailed analysis of these early time points. However, an understanding of early events in particular is essential for the development of preventive therapies, which are urgently needed. Breast cancer brain metastases are thought to develop at a late stage of progressive metastatic disease and ultimately fail to respond to treatment. Therefore, effective therapies for prevention could be lifesaving for patients who are at risk for developing brain lesions.

In the present study, we analyzed the brain microenvironment during the initiation of hematogenous breast cancer brain metastasis, using animal models that allowed us to capture the involvement of different brain-resident cells in this process. We found that cancer cells extravasated exclusively from capillaries. In some cell lines, this step preceded their proliferation and establishment of metastatic foci, whereas other cell lines began to proliferate within the brain microvasculature. However, the timing between tumor cell arrest and extravasation was always the same and required several days. Thus, survival of arrested cancer cells within brain capillaries might be a rate-limiting step in metastatic progression. This might be true specifically for the brain, because cancer cell penetration of the vessel wall in the brain is much slower than in other organs.[13,27] Strikingly, arrest of individual tumor cells in brain capillaries induced diverse astrocytic and microglial responses, even before the tumor cells extravasated. These responses resulted in heterogeneous local changes of the initial tumor microenvironment. We speculate that these changes might influence the fate of individual cancer cells, promoting or restricting their progression into macrometastases. In the future, our models should enable detailed *in vivo* analyses of these early interactions and contribute to the development of preventive therapeutic approaches that target early host responses within the brain microenvironment. Such strategies may hold particular promise because cancer cells may constantly change their phenotype due to genetic instability, in contrast to the more stable host microenvironment. Thus, microenvironment-based therapies might find broader application for different cancer types and affect different stages of progression.

Materials and Methods

In Vivo *Mouse Models, Bioluminescence Imaging, and Tissue Preparation*

MDA-MB-435, MDA-MB-231, MDA-MB-231/brain,[28] 4T1, and MCF-7 cells were grown in Eagle's minimum essential medium supplemented with nonessential amino acids, vitamin mix, L-glutamin, pyruvate, and 10% serum. 4T1 cells were stably transduced with lentiviral green fluorescent protein (GFP)-expressing vector to enable their detection by immunofluorescence. For *in vivo* imaging, all tumor cell lines were stably transduced with Firefly luciferase (F-luc) in a lentiviral construct.[29] F-luc-tagged cancer cells (10^4, 2×10^4, and/or 10^5) were injected into the left internal carotid artery of female BALB/c mice (4T1 cells) or CB17/SCID mice (all other cell lines) in Eagle's minimum essential medium without supplements in a total volume of 50 μl. For surgery, mice were anesthesized with isofluorane. To detect hypoxia, Hypoxyprobe (Natural Pharmaceuticals Inc., Burlington, MA) (150 μl of 10 mg/ml i.p.) was injected into the animals 45 minutes before tissue harvest. The surgery protocol and all animal work were approved by the institutional animal care and use committee (American Association for the Accreditation of Laboratory Animal Care accredited).

Tumor cell arrest and growth within the brain tissue were monitored by repeated noninvasive bioluminescence imaging using an IVIS 200 system (Xenogen, Alameda, CA) after luciferin injection (i.p.). On day 1, 2, 3, 5, 7, 10, and 50 to 70 posttumor cell injection, brain tissue was harvested after perfusing deeply anesthesized animals with 20 ml of 0.9% NaCl, followed by 20 ml of 4% paraformaldehyde in PBS. Isolated brain tissue was post-fixed in 4% paraformaldehyde for 4 to 8 hours at 4°C, then incubated in 25% sucrose/0.1 M sodium phosphate buffer at 4°C overnight, and snap-frozen on dry ice. Brains were cut entirely into 30-μm cryosections, collected in Walter's antifreeze (30% (v/v) ethylenglycol, 30% (v/v) glycerol, and 0.5 M phosphate buffer) and stored at −20°C.

Immunohistochemistry and Immunofluorescence

Before staining, floating sections were washed three times in PBS, treated with 3% H_2O_2/10% methanol in PBS for 15 minutes, blocked in 10% goat serum/0.3% Triton X-100 in PBS for 1 hour, and incubated with primary

antibody (Ab) overnight, followed by incubation with secondary horseradish peroxidase-, alkaline phosphatase-, or biotin-conjugated Abs (Jackson ImmunoResearch Laboratories, West Grove, PA and Vector Laboratories, Burlingame, CA) for 2 hours. For double and triple staining, sections were incubated sequentially with one Ab at a time. Different horseradish peroxidase substrates (diaminobenzidine; BD Pharmingen or Vector-SG, Vector Laboratories) and alkaline phosphatase substrate (Vector-Red; Vector Laboratories) were used to visualize the antigens. Signal from biotinylated Abs was amplified using an avidin-biotin complex kit (Vector Laboratories). After transferring the sections onto glass slides, nuclei were stained with Contrast Green (Kirkegaard & Perry Laboratories, Gaithersburg, MD), and the slides were washed with isopropanol and briefly incubated in Safe-Clear II (Fisher Scientific, Pittsburgh, PA) before mounting in Permount (Fisher Scientific).

For immunofluorescence, secondary Abs conjugated with Alexa 488, Alexa 549, allophycocyanin (APC) (Invitrogen, Carlsbad, CA), tetramethylrhodamine isothiocyanate, or fluorescein isothiocyanate (Jackson ImmunoResearch Laboratories) were used, nuclei visualized with 4′,6′-diamidino-2-phenylindole, and the slides were mounted in Gel Mount (Biomeda, Foster City, CA).

Primary Abs used were anti-CD34 (Abcam, Cambridge, MA), anti-mouse-CD31 (BD Pharmingen), anti-human CD44 (monocloncal Ab (mAb) 29.7),[30] anti-glial fibrillar acidic protein (GFAP) (Promega, Madison, WI), anti-mouse Nestin mAb 353 (Chemicon International, Temecula, CA), anti-matrix metalloproteinase (MMP)-9 (Ab-7, Oncogene Research Products, San Diego, CA), anti-SDF-1 (Santa Cruz Biotechnology), anti-Ki-67 (BD Pharmingen), anti-smooth muscle actin (Sigma-Aldrich, St. Louis, MO), anti-F4/80 (Cederlane Laboratories, Hornby, Ontario, Canada), anti-platelet-derived growth factor receptor β (eBioscience, San Diego, CA), anti-human vimentin (DakoCytomation, Fort Collins, CO), anti-GFP (Chemicon International), anti-mouse GPIb$_\alpha$ (Emfret Analytics, Eibelstadt, Germany), anti-Hypoxyprobe (Natural Pharmaceuticals Inc., Burlington, MA), and anti-fibrin (murine hybridoma HB8545; American Type Culture Collection). BS-1 lectin was from Sigma-Aldrich. The TACS TdT kit (R&D Systems, Minneapolis, MN) was used for terminal deoxynucleotidyl transferase-mediated dUTP nick-end labeling staining.

Images were acquired with a Zeiss Axio Imager M1m microscope equipped with a digital camera, using $\times$10 or $\times$20 air objectives. Digital images were analyzed using AxioVision 4.6 software (Zeiss, Oberkochen, Germany). Confocal images were acquired with an Olympus IX81 microscope equipped with UltraVIEW VoX Confocal Imaging System (PerkinElmer, Wellesley, MA), using a $\times$40 water immersion objective. Images were acquired and analyzed using the Velocity software.

Quantification of Tumor Cell Extravasation

To detect the tumor cells, tissues were stained with anti-GFP Ab (4T1), anti-human CD44 (mAb 29.7), or human vimentin (human cell lines) and costained with anti-CD31 to visualize the vascular endothelium. The position of the tumor cells inside or outside blood vessels was determined for each detected tumor cell. For MDA-MB-435 cells, every fourth section throughout the entire brain was analyzed. At each time point (days 3, 5, and 7), $n = 4$ brains were examined. On day 3, we found 253, 130, 90, or 301 tumor cells per brain, respectively, and 15, 16, 48, or 196 tumor cells on day 5. For MDA-MB-231/brain and 4T1 cells, 60 randomly chosen events in each of two to three different animals were examined per time point. The percentage of intravascular versus extravascular tumor cells was calculated.

The gross quantification was performed using images acquired with Zeiss Axio Imager M1m microscope, which allowed for quantification of a large number of events. For a subset of events, the localization of cancer cells inside or outside the vasculature was confirmed by confocal microscopy.

Quantification of Ki-67-Positive Cells

Tissue was costained for Ki-67 and human CD44 (MDA-MB-435) or human vimentin (MDA-MB-231/brain). Every fourth section of the entire brain was analyzed in two to three different animals 30 to 50 days postinjection. The number of Ki-67-positive and -negative cells was counted for solitary cancer cells and for metastatic lesions containing >30 cells. For each of these lesion types, the percentages of Ki-67-positive cells were calculated. SDs and statistical significance were determined by two-tailed Student's *t*-test.

Quantification of Astrocyte Association with Cancer Cells

Three days after injection of cancer cells into the carotid artery, the brain tissue was stained for GFAP to detect astrocytes and costained for human CD44(435), human vimentin (231/brain), or GFP (4T1) to detect the cancer cells. The number of reactive astrocytes located within a distance of 150 μm from the cancer cells (cancer cell associated) and the number of reactive astrocytes in the corresponding area of the nonafflicted contralateral hemisphere (normal control) was counted for 20 randomly chosen events per brain in two to three animals for each cancer cell line. SDs and statistical significance were determined by two-tailed Student's *t*-test.

Results

Models and Kinetics of Initial Cancer Cell Colonization of the Brain

To define models suitable for studying the earliest steps of cancer cell brain colonization, we injected five different F-luc-tagged breast cancer cell lines into the left internal carotid artery of female immunodeficient or immunocompetent mice and followed cancer cell distribution and

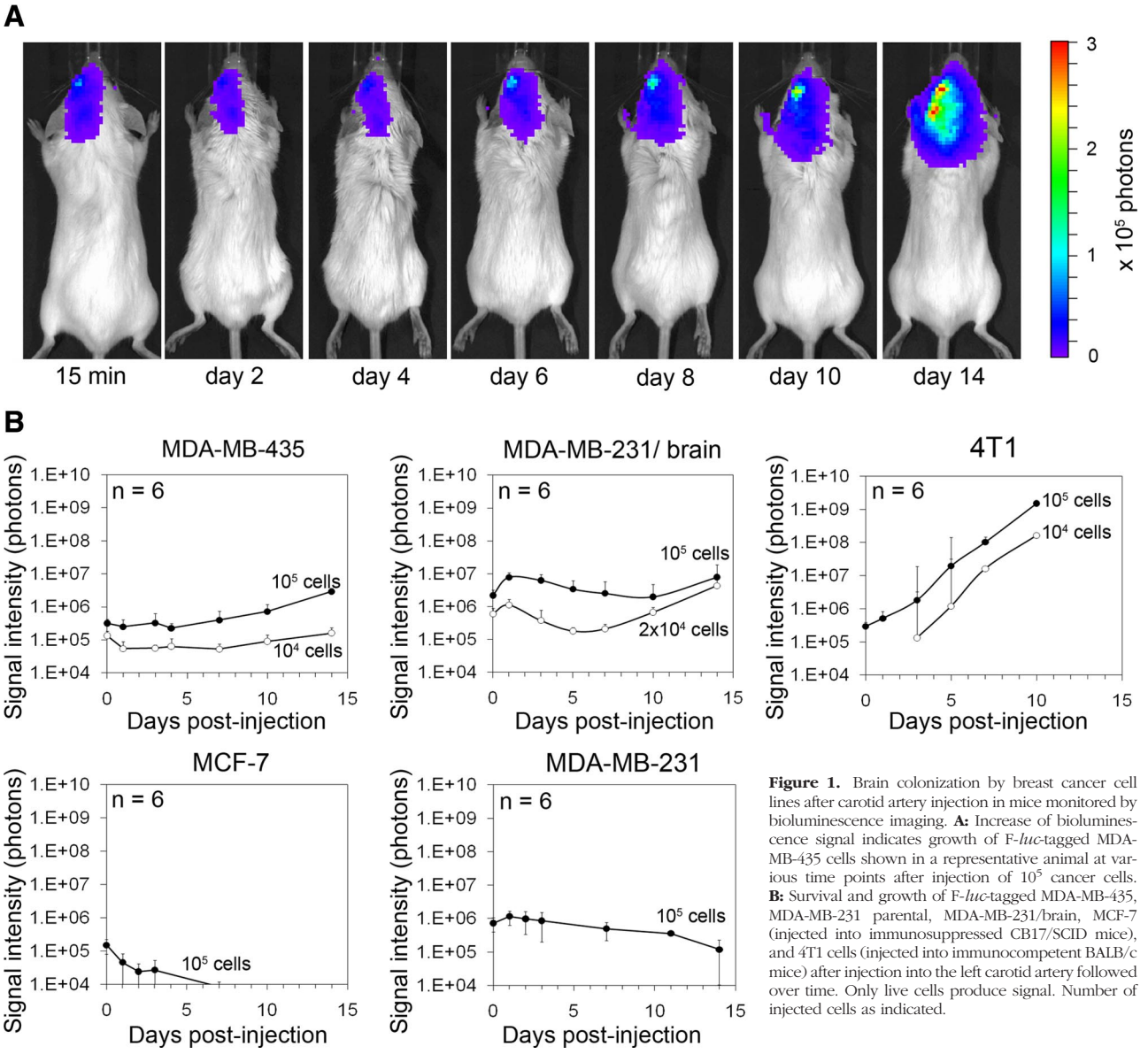

Figure 1. Brain colonization by breast cancer cell lines after carotid artery injection in mice monitored by bioluminescence imaging. **A:** Increase of bioluminescence signal indicates growth of F-*luc*-tagged MDA-MB-435 cells shown in a representative animal at various time points after injection of 10^5 cancer cells. **B:** Survival and growth of F-*luc*-tagged MDA-MB-435, MDA-MB-231 parental, MDA-MB-231/brain, MCF-7 (injected into immunosuppressed CB17/SCID mice), and 4T1 cells (injected into immunocompetent BALB/c mice) after injection into the left carotid artery followed over time. Only live cells produce signal. Number of injected cells as indicated.

growth by noninvasive bioluminescence imaging (Figure 1). CB17/SCID mice were used to analyze human tumor cells and BALB/c mice for syngeneic murine 4T1 breast cancer cells. Comparing MDA-MB-435, MDA-MB-231, MDA-MB-231/brain,[28] MCF-7, and 4T1 cells, we found that all five cell lines were detectable within the brain area 15 minutes postinjection. Even though each of these cell lines initially localized to the brain area, only MDA-MB-435, MDA-MB-brain/brain, and 4T1 cells produced persistent and increasing signal over time, whereas MDA-MB-231 parental and MCF-7 signal declined and eventually disappeared (Figure 1, A and B). Immediately after carotid artery injection of 10^4 or 10^5 MDA-MB-435 cells, strong bioluminescence signal was detected in the left hemisphere of the brain and the signal persisted without major change in intensity through days 5 to 7, before it increased continuously (Figure 1, A and B). Only live cells produce signal, indicating that the majority of the initially arrested cancer cells remained and survived this step. Just after carotid artery injection of MDA-MB-435 cells, a weak tumor cell signal was occasionally seen in the lungs, but this signal disappeared within a few days and never reappeared (data not shown). The signal for MDA-MB-231/brain cells initially decreased slightly, indicating that some of the cancer cells were eliminated. Between days 5 and 10, the remaining signal then began to increase continuously. 4T1 murine breast cancer cells colonized the brain much more aggressively than the two human cell lines. The 4T1 signal started to increase immediately after tumor cell injection and continued to increase at a much faster rate than that of MDA-MB-435 and 231/brain cells.

To investigate the behavior of the bioluminescence producing tumor cells in more detail, we followed individual cells by histology on days 3, 5, and 7. We analyzed the entire brain of each animal by immunohistochemistry at each of these time points (n = 2–4 mice per time and cell type). Human tumor cells were detected using two

independent markers (human CD44 and human vimentin). Murine 4T1 cells were identified by their GFP label via anti-GFP staining. We found that MDA-MB-231 parental cells were rapidly cleared from the circulation of the brain parenchyma and were undetectable inside or outside the vasculature of the brain tissue on days 3, 5, and 7 postinjection. Residual bioluminescence signal of MDA-MB-231 parental cells in the brain area seen through day 5 (Figure 1) was likely due to tumor cells in the leptomeninges, which remained attached to the skull when the brains were removed for histology at these early time points. In contrast, MDA-MB-435, MDA-MB-231/brain, and 4T1 cells were readily detected throughout the brain parenchyma very early (eg, days 1, 2, 3, and 7) as well as at later time points. After 10 to 50 days, numerous macrometases were found in 100% of the animals (n = 3–6/group) after injecting 10^4 to 10^5 of these tumor cells. 4T1 cells exhibited the most rapid growth in their immunocompetent hosts and produced extensive metastatic burden already after 10 days. MDA-MB-435 and brain homing MDA-MB-231/brain cells were previously reported to produce metastatic lesions in the brain when administered into the bloodstream,[28,31] but the early colonization steps have not been previously investigated. MDA-MB-435 cells are aggressively metastatic breast cancer cells that share some characteristics with melanoma,[32,33] another tumor type that frequently causes brain metastasis in patients.[1] The MDA-MB-231/brain cell line was derived from MDA-MB-231 parental breast cancer cells after cardiac injection into immunodeficient mice and six cycles of isolating brain metastases and reinjection into the heart.[28] Here, we demonstrated that MDA-MB-231/brain cells, as well as MDA-MB-435 and 4T1 cancer cells, are suitable models for studying cancer cell interaction with the brain microvasculature even at the earliest time points, for following the ability of cancer cells to survive and grow within the brain tissue, and for analyzing involved host cell responses.

Cancer Cell Extravasation, Growth in the Brain, and Types of Blood Vessels Involved

To analyze the mode and timing of cancer cell extravasation, their initial proliferation in the brain parenchyma, and the types of blood vessels involved in extravasation and lesion growth, we followed the cancer cells on days 1, 2, 3, 5, and 7 after carotid artery injection by immunohistochemistry.

The localization of cancer cells and blood vessels was determined by staining the human cancer cells with anti-human CD44 (mAb 29.7)[30] or anti-human vimentin, mouse 4T1 cells with anti-GFP, and the vasculature with anti-CD31 (Figure 2, A–G, and Supplemental Figure 1, see *http://ajp.amjpathol.org*). During the first 2 days after inoculation, all cancer cells were found inside blood vessels and displayed an elongated shape to fit into the narrow capillaries (Figure 2A). On day 3 postinoculation, for all three cell lines examined, the majority of cancer cells were still localized within the microvasculature (Figure 2, B, H, and I, and Supplemental Figure 1, see *http://ajp.amjpathol.org*). Only a small percentage was extravasating (Figure 2, C, H, and I, and Supplemental Figure 1, see *http://ajp.amjpathol.org*) or already located in the extravascular space, staying close to the vessels from which the cells had emerged (Figure 2D and Supplemental Figure 1, see *http://ajp.amjpathol.org*). Before or during extravasation, the cancer cells rounded up inside the vascular lumen and formed cytoplasmic protrusions, which apparently expanded the vessel wall that surrounded them (Figure 2B; also see Figure 5C, day 3, blue arrowheads). Intravascular cancer cells penetrating the blood vessel wall with their cytoplasmic protrusions were also detected (Figure 2I, middle panel, and Supplemental Figure 1, see *http://ajp.amjpathol.org*). Extravasation of individual cancer cells seemed to at least occasionally involve larger interruptions of the vessel wall (Figure 2, C–F). However, we could not detect any apoptosis or hypoxia associated with the endothelium at sites of cancer cell extravasation by terminal deoxynucleotidyl transferase-mediated dUTP nick-end labeling staining or hypoxyprobe, respectively. This suggests that the extravasation events were not associated with significant destruction of the vessel wall (data not shown). However, fibrin formation and platelet aggregation were detected at sites of 4T1 cell extravasation in BALB/c mouse brain on days 3, 5, and 7 posttumor cell injection (Figure 2J and data not shown). On day 5 postinoculation, 20 to 40% of the cancer cells were still intravascular (Figure 2H). On day 7, all MDA-MB-435 and 4T1 tumor cells were found in the extravascular space, whereas ~15% of MDA-MB-231/brain cells were still intravascular, suggesting a slightly slower extravasation kinetics (Figure 2, E–I, and Supplemental Figure 1, see *http://ajp.amjpathol.org*). At this time, for all three cell lines, small groups of cancer cells were detected close to capillaries or lined up along the vessel wall at the parenchymal side, indicating initial cancer cell growth (Figure 2, F and G, and Supplemental Figure 1, see *http://ajp.amjpathol.org*). Notably, for MDA-MB-435 cells, extravasation always preceded cancer cell proliferation, because groups of two or more cancer cells were seen only in the extravascular space and never inside blood vessels (Figure 2, C–G). In contrast, groups of cancer cells within the vasculature were found for 4T1 cells, suggesting that these cells might proliferate even before extravasating. This is in line with the immediate increase in bioluminescence signal for this cell line from day 1 on (Figure 1B).

By days 30 to 70, all mice injected with MDA-MB-435 or MDA-MB-231/brain cells harbored large metastatic lesions within the brain parenchyma and leptomeninges. At this stage, leptomeningeal metastases remained attached to the brain surface when the brains were harvested, allowing us to analyze these lesions in detail and to compare them to lesions within the brain tissue. Although metastases in the brain parenchyma grew preferentially around capillaries, forming elongated clusters around these small vessels (Figures 2K and 3C), leptomeningeal lesions were compact nodules and contained capillaries as well as larger vessels (Figure 3C).

Because of the rapid intracranial growth of 4T1 cells, these experiments were terminated after 10 to 14 days.

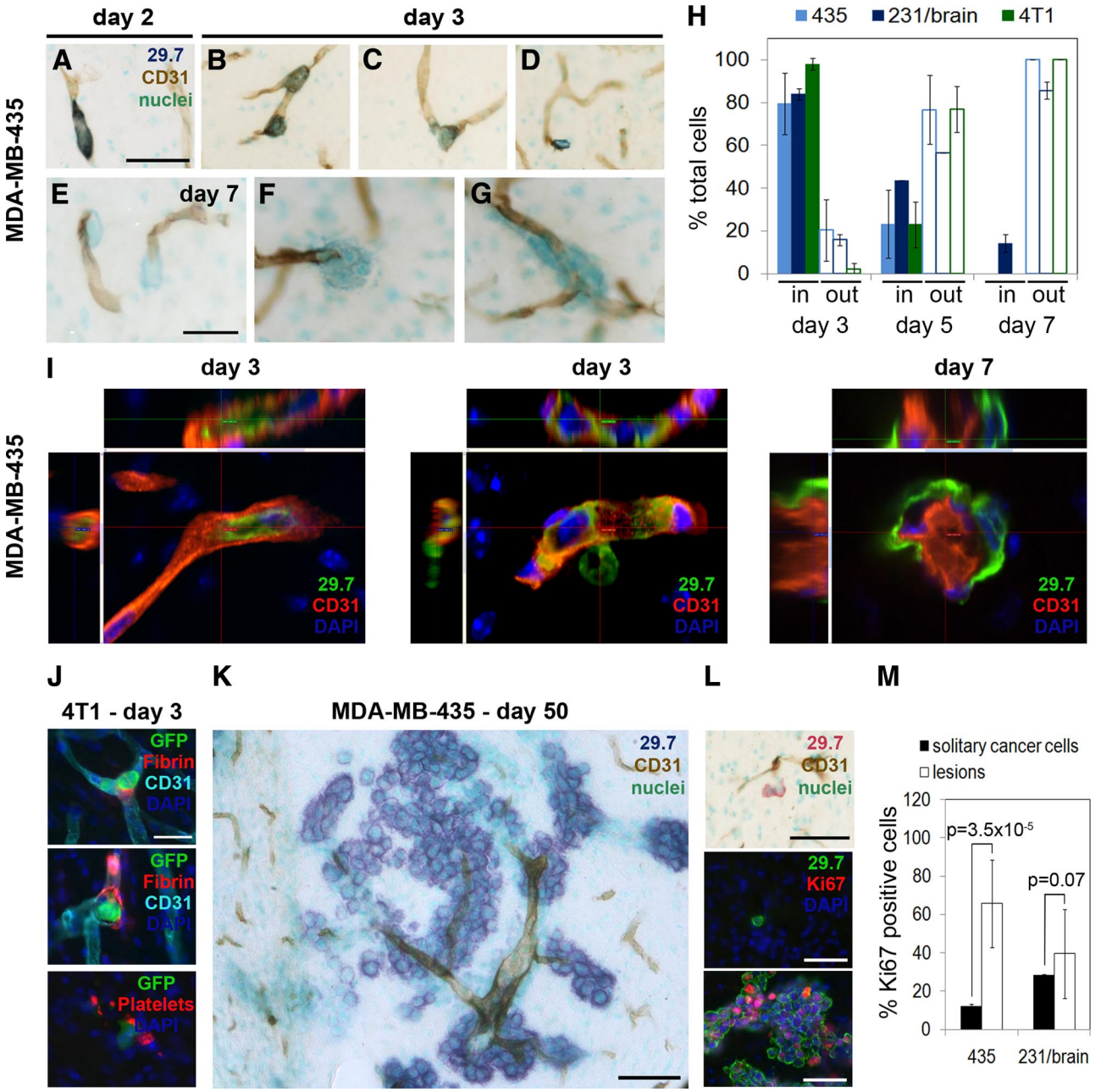

Figure 2. Cancer cell extravasation and growth in the brain. **A–G:** MDA-MB-435 cells were visualized by anti-human CD44 (mAb 29.7) and blood vessels by CD31 staining using immunohistochemistry. **A:** An elongated cancer cell within a capillary on day two postinjection. **B:** Rounding of intravascular cancer cells on day three. **C:** Cancer cell on day three breaking through the vessel wall during extravasation. **D:** Extravasated cancer cell on day three. **E–G:** Extravascular cancer cells on day seven. Scale bars: 50 μm (**A–D**); 25 μm (**E–G**). **H:** Percentage of cancer cells located inside versus outside blood vessels. The quantification was performed for three different cells lines: MDA-MB-435, MDA-MB-231/brain, and 4T1. **I:** Analysis of early cell location by confocal microscopy. Cancer cells were stained for human CD44 (green) and blood vessels for CD31 (red). An intravascular cell (**left panel**), a cell in the process of extravasation (**middle panel**), and extravascular cells (**right panel**) are shown. **J:** Association of intravascular 4T1 cancer cells with fibrin and platelets ($GPIb_{\alpha}$ staining) on day three. Scale bar: 25 μm. **K:** Day 50: Long-term fate of MDA-MB-435 cells was monitored by immunohistochemistry. Intraparenchymal macrometastases grew preferentially around co-opted blood vessels. Scale bar: 200 μm. **L:** Solitary tumor cells outside blood vessels on day 50 (**top panel**), detected by anti-human CD44 (mAb 29.7), are mostly negative for Ki-67 (**middle panel**). In contrast, most cells within lesions as shown in **K** are Ki-67 positive (**bottom panel**). Scale bars: 50 μm. **M:** Quantification of Ki-67-positive cells within the solitary cancer cell population and within the macrometastatic lesions for MDA-MB-435 and MDA-MB-231/brain cells 30 to 50 days postinjection.

All animals harbored numerous macrometastases, tightly lined up along blood vessels within the brain parenchyma. No obvious leptomeningeal lesions were observed for this cell model.

During the initial steps of brain colonization within the parenchyma, cancer cells exclusively arrested within and extravasated from capillaries and/or postcapillary venules. These vessels were identified by immunohistochemistry based on their size and lack of smooth muscle cells (Figure 3A). The vessels were positive for CD31 as well as for CD34 and were surrounded by platelet-derived growth factor receptor β-positive peri-

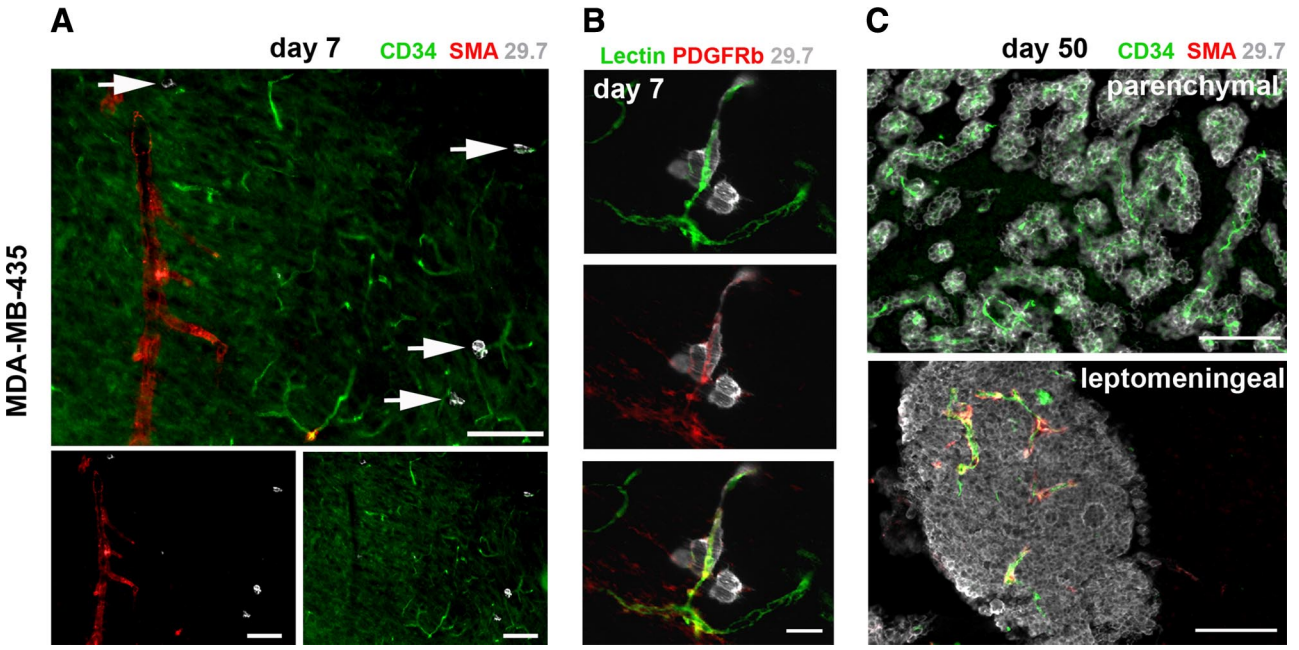

Figure 3. Blood vessel types involved in cancer cell extravasation and growth. Blood vessel types were analyzed by immunofluorescence. Representative images for MDA-MB-435 cells are shown. **A:** Day seven: in the brain parenchyma, cancer cells (white, **arrows**) arrest and extravasate exclusively from capillaries or postcapillary venules positive for CD34 and lacking smooth muscle cells (no smooth muscle actin (SMA) signal). Scale bars: 100 μm. **B:** Day seven: blood vessels from which cancer cells (gray) extravasate are surrounded by platelet-derived growth factor receptor β (PDGFRb)-positive pericytes. **Top panel:** BS-1 lectin; **middle panel:** anti-PDGFRb; and **bottom panel:** merge. Scale bar: 20 μm. **C:** Day 50: intraparenchymal metastases grow around co-opted capillaries lacking smooth muscle cells. Leptomeningeal metastases contain capillaries as well as larger, smooth muscle cell-positive vessels. Scale bars: 100 μm.

cytes (Figure 3B). This indicates that parenchymal lesions stayed associated with the vessel type from which they initially emerged.

In addition to successfully growing large metastatic lesions, we detected many single cancer cells scattered throughout the brain at late time points for MDA-MB-435 and 231/brain cell models (days 30 to 70 postinjection). These cells were localized within the brain parenchyma next to capillaries (Figure 2L, top panel). The majority of the solitary MDA-MB-435 cancer cells were not proliferating, as only 12% of these cells were positive for cell cycle marker Ki-67 (Figure 2, L, middle panel, and M). Thus, these solitary cancer cells were arrested in G_0 of the cell cycle and remained dormant after extravasation, whereas the majority of cancer cells within larger lesions (63%) were Ki-67 positive and proliferated actively (Figure 2, L, bottom panel, and M). In contrast, there was no significant difference in the percentage of Ki-67-positive cells between the solitary cancer cell population and macroscopic lesions for MDA-MB-231/brain cells (Figure 2M). Notably, no solitary cancer cell population was detected for the aggressive murine 4T1 breast cancer cell line in their syngeneic BALB/c host model. All observed 4T1 cells grew in tight clusters around blood vessels 10 days after carotid artery injection (data not shown).

Cancer Cell Arrest and Extravasation in the Brain Induce Diverse Microglial and Astrocyte Responses

It is well established that the host microenvironment affects tumor growth and metastatic progression and impacts the success of tumor cells to survive and grow within the brain.[6,29,34–36] Therefore, we investigated the earliest responses of brain residing cells to incoming cancer cells during the initial steps of hematogenous brain metastasis. A major cell type of the brain known to respond to invading cells from the immune system during inflammatory brain disease and development of primary brain tumors is microglia.[14–18] We therefore investigated an involvement of microglia in the earliest steps of cancer cell brain colonization. F4/80 was used as a marker for microglia and macrophages. Our analysis revealed a varying accumulation of F4/80-positive cells with strongly increased F4/80 expression, indicative of microglial activation, around extravasated cancer cells on day 7 in all three cancer cell models (MDA-MB-435: Figure 4A–G; 4T1: Figure 4H-K; MDA-MB-231/brain: data not shown). Similar microglial responses were observed in immunosuppressed SCID mice and immunocompetent BALB/c mice. Some cancer cells that had left the vasculature recruited large amounts of activated microglia, whereas only few or no activated microglial cells could be detected in the vicinity of other cancer cells (Figure 4, A and H, left panel). However, the microglial responses observed were specifically induced by the cancer cells, and were not a consequence of the surgical manipulation since activated microglial cells were never detected in the same brain regions of animals injected with medium alone (Figure 4H, right panel). Microglia associated with the initial micrometastases presented either as activated microglia displaying characteristic stellate morphology with thick cellular processes (Figure 4, D and J) or as reactive microglia with typical amoeboid morphology[37]

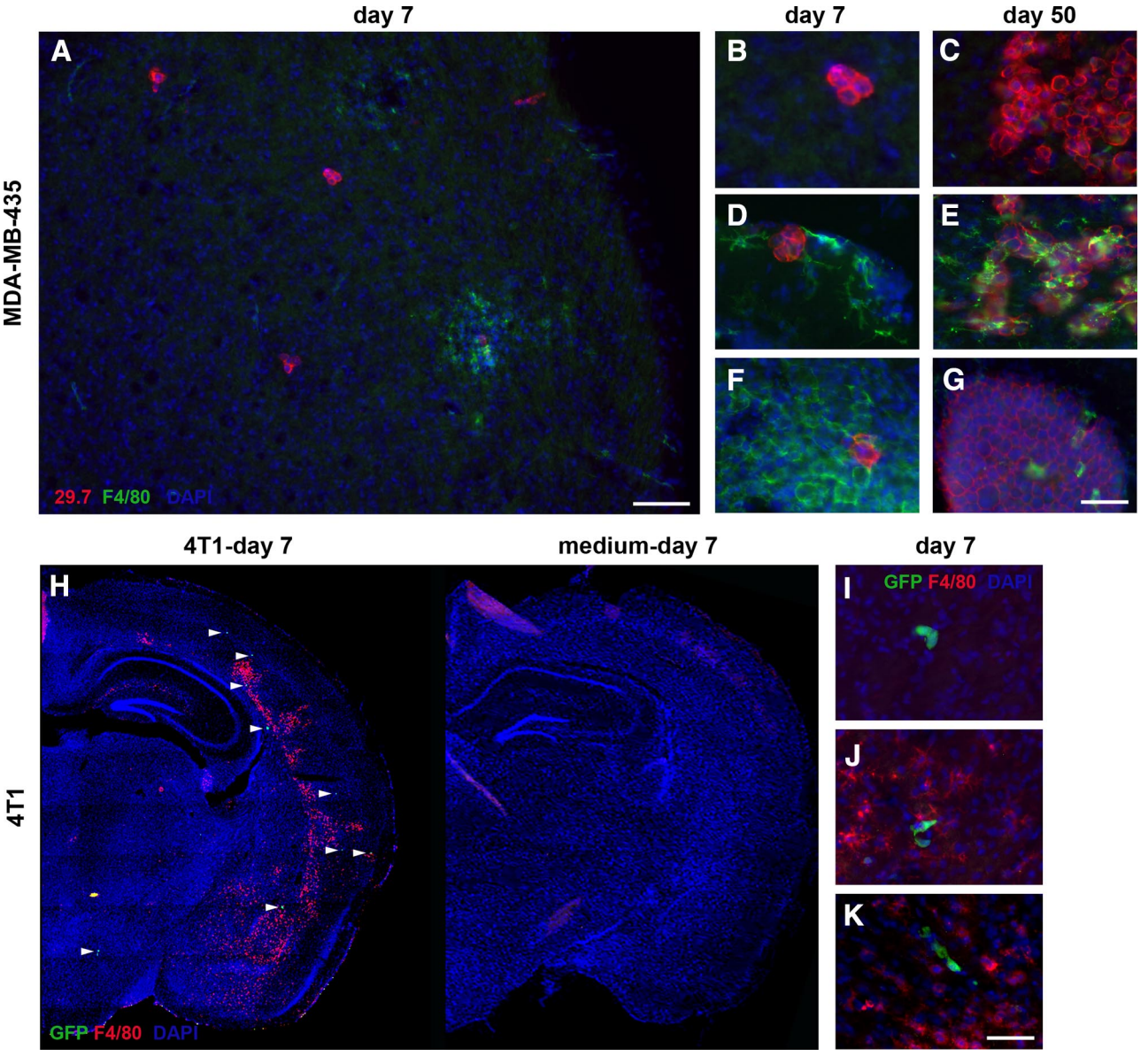

Figure 4. Microglial cell responses to invading cancer cells are heterogeneous. Microglial activation in response to cancer cell invasion varies at early as well as late stages, as detected by immunofluorescence analysis. **A–G:** MDA-MB-435 cells in immunosuppressed mice; diverse microglial responses (green) to incoming cancer cells (red) on day seven (**A**). Responses include absence of microglial cells (**B**), presence of hypertrophic stellate activated (**D**), or amoeboid reactive microglial cells (**F**). Similarly, on day 50, some macrometastases show no microglial involvement (**C**) or contain stellate (**E**) or amoeboid microglia (**G**). Scale bars: 100 μm (**A**); 50 μm (**B–G**). **H–K:** 4T1 cells in immunocompetent mice; **H:** distribution of activated microglia (red) in the mouse brain seven days after carotid artery injection of cancer cells (**left panel**) or medium alone (**right panel**). **White arrowheads** mark the GFP-labeled cancer cells (green). Diverse microglial responses to cancer cells include absence of microglial cells (**I**), presence of hypertrophic stellate (**J**), or reactive amoeboid microglial cells (**K**). Scale bar: 50 μm.

(Figure 4, F and K). The heterogeneity in microglial responses persisted throughout metastatic lesion development. Even macrometastases on day 50 posttumor cell injection were either completely free of microglial cells (Figure 4C) or found associated with activated stellate (Figure 4E) or reactive amoeboid microglia (Figure 4G). Thus, microglial responses to brain invading cancer cells can generate a variety of local microenvironments that may affect lesion growth. These responses could be dynamically regulated, potentially explaining their sporadic detection.

In addition to the variable microglial responses, astrocytes and their activation were consistently found associated with invading cancer cells from the earliest intravascular arrest steps on (Figure 5). In addition to pericytes, brain capillaries are supported by astrocytes, which contribute to the tightness and functions of the blood-brain barrier.[38–40] After interacting with endothelial cells, pericytes and astrocytes are the first host cell types that extravasating cancer cells encounter. Strikingly, in all three cancer cell models, arrest and extravasation of cancer cells consistently resulted in a strong local activation of astrocytes, detected by the up-regulation of GFAP as well as by the hyperdilation of astrocyte processes (MDA-MB-435: Figure 5, A and C; 4T1: Figure 5D; MDA-MB-231/brain: data not shown).

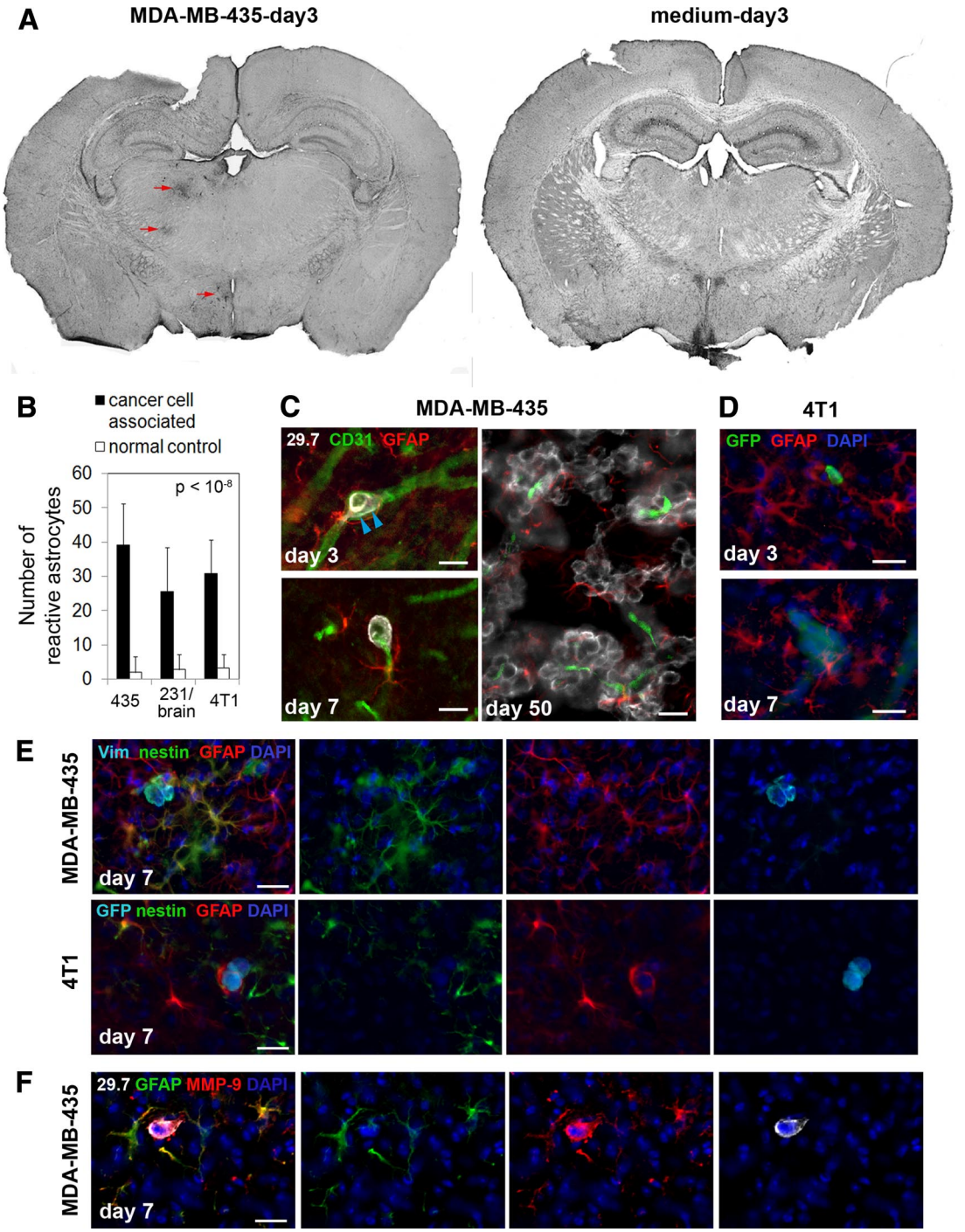

Figure 5. Cancer cell invasion induces strong astrocytic responses. Astrocytes were investigated by immunofluorescence staining. **A: Left,** On day three after cancer cell injection into the left carotid artery, GFAP in astrocytes is already up-regulated strongly in the vicinity of intravascular arrested cancer cells (MDA-MB-435, **red arrows**). Astrocyte activation can be detected in the left hemisphere in brain overview sections, whereas the corresponding area of the contralateral hemisphere is devoid of GFAP reactivity. **Right,** Also, no GFAP activity was found in the brain of control animals injected with medium alone. **B:** Number of reactive astrocytes three days after carotid artery injection of cancer cells, quantified within the 150-μm distance from cancer cells (cancer cell associated) and within the corresponding region of the contralateral hemisphere that lacks cancer cells (normal control). **C:** Activated astrocytes with thick processes and up-regulated expression of GFAP are detected next to MDA-MB-435 cancer cells that are still intravascular. Note the cytoplasmic protrusions of cancer cells on day three postinoculation that apparently cause stretching of the vessel wall (**blue arrowheads**) (day three, **upper left panel**). GFAP-positive astrocytes stay close to extravasated tumor cells (day seven, **lower left panel**). Reactive astrocytes persist close to cancer cells throughout their development into macrometastases (day 50, **right panel**). Scale bars: 20 μm. **D:** Activated astrocytes are also present in the vicinity of 4T1 breast cancer cells injected into the carotid artery of syngeneic BALB/c mice. Scale bars: 20 μm. **E:** In addition to GFAP up-regulation, some reactive astrocytes simultaneously express nestin. Merged images are shown on the **left**. Human vimentin or GFP (light blue), nestin (green), GFAP (red), and 4′,6′-diamidino-2-phenylindole (DAPI) (dark blue). Scale bar: 20 μm. **F:** Strong up-regulation of MMP-9 is detected in reactive astrocytes located in the immediate vicinity of extravasated MDA-MB-435 tumor cell. Scale bar: 20 μm.

Astrocyte activation was always and exclusively seen in close proximity of cancer cells. In many cases, the astrocyte response was so strong that it could be detected in overviews of whole brain sections, even on day 3 post-cancer cell injection (Figure 5A). At this stage, reactive astrocytes were present in close proximity of individual cancer cells, even before those extravasated (Figure 5C, day 3). Reactive astrocytes persisted throughout the extravasation process (Figure 5, C and D, day 7) and establishment of large metastatic lesions (Figure 5C, day 50). Early astrocyte activation on day 3 was a specific response to the presence of cancer cells, because the injection of medium alone in sham operated animals did not result in any detectable astrocyte activation (Figure 5A). Furthermore, no increase in reactive astrocytes was observed for the corresponding brain area in the contralateral brain hemisphere (Figure 5A). Notably, injection of breast cancer cells into the left internal carotid artery resulted in tumor cell colonization of only the left hemisphere of the brain, whereas the right hemisphere remained unaffected. We therefore used the right tumor cell-free hemisphere as a control to quantify the number of reactive astrocytes associated with cancer cells in the left hemisphere. The results demonstrate a significant and specific increase in reactive astrocytes in the proximity of cancer cells on day 3 postinjection for all three breast cancer cell models (Figure 5B).

In addition to elevated expression of GFAP, some cancer cell-associated astrocytes simultaneously up-regulated expression of nestin, another marker of reactive astrocytes[41] (Figure 5E). We confirmed that nestin staining was truly associated with astrocytes by costaining blood vessels and microglia with nestin (Supplemental Figure 2, see *http://ajp.amjpathol.org*). This result reflects a diversity of atrocytic responses to tumor cells.

An important consequence of astrocyte activation is their ability to secrete factors such as MMP-9.[42,43] MMP-9 can directly impact cancer cell invasion and has known proangiogenic and growth-promoting functions in brain tumors through release of growth factors from the extracellular matrix.[34] We found a strong expression of MMP-9 by MDA-MB-435 cells as well as a strong up-regulation of MMP-9 protein in the immediate vicinity of extravasating cancer cells, associated with activated astrocytes that surrounded the tumor cells (Figure 5F). Another factor also known to be released by reactive astrocytes is SDF-1,[44–47] but we did not detect SDF-1 in the context of astrocyte responses to cancer cell invasion (data not shown). Taken together, astrocytes might provide early and continuous proangiogenic and/or survival signals that support cancer cell growth. The mechanism might involve release of MMP-9 into the immediate proximity of the cancer cells. Because of their consistent and very early response to arriving cancer cells in the brain and the persistence of their association with proliferating tumor cells, astrocytes might provide a supportive microenvironment for the development of brain metastatic lesions.

Discussion

The present study provides detailed *in vivo* analyzes of breast cancer cell arrest and extravasation into the brain parenchyma. Furthermore, it captures the diversity of early host responses within the brain microenvironment during the initial steps of cancer cell invasion. Information on the first interaction between brain-homing tumor cells and reactive host cell types will contribute to a better understanding of critical early events in brain metastasis. This insight may help develop strategies for prevention and treatment of symptomatic brain lesions.

Our results show that breast cancer cells arrest exclusively in brain capillaries and/or postcapillary venules. Comparing five different breast cancer cell models, we identified three as suitable models for detailed studies of the earliest critical events of breast cancer cell extravasation and initial brain colonization. Importantly, only these tumor cells consistently developed metastatic lesions. Reports in the literature differ on the time course of cancer cell extravasation, likely because of the use of different cancer cell types, routes of inoculation, and primarily because of distinct microvascular structures within the target organs examined. In general, it takes significantly longer for cancer cells to extravasate into the brain parenchyma than into other organ tissues. For example, extravasation of lung cancer cells in the brain was reported to take 48 hours, whereas the same tumor cells extravasated into the liver within only 6 hours.[13] In another study, prostate cancer cells derived from brain metastases apparently remained inside brain capillaries for up to 5 days.[27] In our approach, breast cancer cells were injected into the left internal carotid artery of immunosuppressed SCID mice or immunocompetent BALB/c mice. Importantly, we found that regardless of the host immune state, the timing of tumor cell arrest within the vasculature and extravasation was the same for all tumor cell models examined. We found the tumor cells arrested within the brain microvasculature and in the process of extravasation from day 3 on. Extravasation was completed on day 7, except for MDA-MB-231/brain cells, where a small percentage of cells was still intravascular. Thus, arrested cancer cells apparently have to survive within the brain vasculature for a significantly longer period of time than in other organs. Cancer cell survival in the vasculature is likely a critical step that limits the success rate of brain metastasis. This step is probably influenced by the ability of cancer cells to specifically interact with components of the vessel wall on arrest. In line with this concept, it was recently reported[27] that the majority of DU145/RasB1 prostate cancer cells, which arrested in the brain vasculature, were eliminated before they could extravasate, pointing at intravascular survival as a rate limiting step. These studies were performed in immunodeficient mice. The presence of a fully competent immune system, especially natural killer cells,[48] is expected to pose additional survival pressure on cancer cells that remain arrested within the vasculature for extended periods of time. However, our results indicate that arrested breast cancer cells can survive for several days within the cerebral microvasculature in the presence of a

fully functional immune system. We found that 4T1 cells injected into BALB/c mice initiated growth very rapidly without any signs of cancer cell death by terminal deoxynucleotidyl transferase-mediated dUTP nick-end labeling staining (data not shown). In this model, we observed platelet accumulation and fibrin formation associated with intravascular cancer cells, potentially protecting them from the immune system.

Compared with the brain, intravascular survival may be less critical in other organs because of significantly shorter extravasation times. Recently, Bos et al[49] identified genes that promote breast cancer brain metastasis through a gene profiling analysis. Importantly, these genes make up a group of mediators of cancer cell extravasation in an *in vitro* model of the blood-brain barrier. Notably, the duration of transendothelial migration by cancer cells *in vitro* is significantly shorter (6 to 18 hours) than that required for extravasation into brain tissue *in vivo* (3 to 5 days). Furthermore, conditions in the vasculature are much more complex than can be recapitulated *in vitro*. Although one can envision extravasation as a rate-limiting step for cancer types that are able to survive after arresting within the cerebral microcirculation, our results indicate that survival factors—in addition to mediators of extravasation—likely play a decisive role in the establishment of brain metastases.

Different modes of cancer cell extravasation have been described. These include extravasation of individual tumor cells without observable disruption of the microvasculature as well as intravascular cancer cell proliferation, followed by eventual vessel rupture, as reported for lung metastasis.[50–53] In the MDA-MB-435 model, we observed individual cancer cells within brain capillaries that initially assumed an elongated shape to fit into the significantly smaller vessels. Three days later, the tumor cells regained a round shape, thereby stretching the vessel wall. In some cases, the vessels appeared disrupted on extravasation. However, the absence of any detectable apoptosis or hypoxia associated with the vascular endothelium at these sites suggests that no significant damage of blood vessels occurs during the extravasation process. Notably, we also observed cancer cell protrusions stretching through the vessel wall, indicating that crossing of the blood-brain barrier is an active, specific process initiated by the tumor cells. For MDA-MB-435 cells, we did not observe any intravascular proliferation. Groups of two or more cells appeared only in the extravascular space from day 5 on. Consistent with the histology, bioluminescence signal intensity reflecting the number of F-luc-tagged cancer cells started to increase between days 5 and 7 when all of the cells had extravasated. In contrast, we observed intravascular groups of cells for both MDA-MB-231/brain and 4T1 cells, indicating that these might proliferate before extravasation. This finding correlates with the strong, immediate increase in bioluminescence signal for both MDA-MB-231/brain and 4T1 cells within the first day after injection. For MDA-MB-231/brain cells, the signal intensity decreased after day 1, before it began to increase continuously between days 5 and 10, indicating that cancer cells were eliminated from the brain vasculature between days 2 and 5. Exit of cancer cells from capillaries or postcapillary venules may involve mechanical forces caused by rounding of the cancer cells, formation of cytoplasmic protrusions, and most likely secretion of disruptive enzymes such as MMP-9 and heparanase or their combinations.[6,12,36,54] To our knowledge, only one study previously captured cancer cells in the process of extravasation into the brain, using a rat hepatoma cell line as a model.[12] In that model, extravasation apparently involved breaching or destruction of the endothelium. The results from our study with breast cancer cells suggest that different modes of extravasation for cancer cells in the brain might exist.

As lesions progressed, we observed macrometastases within the brain parenchyma as well as in the leptomeninges. These locations represent distinct microenvironments within the brain,[7,36] which we found reflected by strikingly different phenotypes of parenchymal versus leptomeningeal metastases in our models. Throughout their development, metastases in the parenchyma grew mostly around small blood vessels similar to a phenotype reported previously.[9,11,27,55] We identified these vessels as capillaries or postcapillary venules based on their size and lack of smooth muscle cells. In contrast, metastases in the leptomeninges grew into dense solid lesions that always contained larger vessels surrounded by smooth muscle cells. Because of the fragility of the leptomeninges and their tendency to stay associated with the skull when the brains were removed early after cancer cell injection, our analysis of the initial colonization events focused on the parenchymal microenvironment. It is possible that the first steps of cancer cell arrest and extravasation within leptomeninges differ from the events seen within the brain parenchyma.

The brain is a very specialized environment with a unique cellular composition. Recent evidence suggests that adhesion of cancer cells to components of the vascular basement membrane provides essential survival cues for cancer cells, early during brain colonization.[9] In addition to initial signals from tumor cell adhesive interactions with the vessel wall, host cells in the immediate microenvironment of the tumor cells are most likely to impact their fate and ability to progress. In our study, we focused on host cell responses to the invading tumor cells. For established brain metastases, it has been well documented that reactive astrocytes and microglia surround the lesions.[15,22] Furthermore, it is known that glial cells are activated in a response to brain injuries. However, responses of glial cells and astrocytes to the initial stages of tumor cell invasion have not been reported previously. We found that cancer cell arrest, extravasation, and invasion of the brain parenchyma always induced a strong local activation of astrocytes and activation of microglia to varying degrees. Astrocytic responses were heterogeneous in their intensity and cellular composition, involving cells with up-regulated expression of GFAP, nestin, or both. Reactive astrocytes occasionally strongly up-regulated expression of MMP-9, which is known to promote growth of primary brain tumors based on its proangiogenic activity by releasing vascular endothelial growth factor from the surrounding matrix.[34] In addition, vascular endothelial growth factor can also

directly stimulate the proliferation of cancer cells.[56] Furthermore, astrocytes were shown to support brain metastatic growth by secretion of heparanase[24] and neurotrophins.[23] Thus, reactive astrocytes may provide initial cues for extravasating tumor cells to survive and proliferate within the brain parenchyma.

Some reactive astrocytes in the vicinity of cancer cells expressed nestin. Nestin is a marker of neuroepithelial stem cells, radial glia cells, and progenitor cells and is down-regulated during terminal differentiation to mature astrocytes. Nestin up-regulation in reactive astrocytes was found associated with brain injury from different causes.[41,57–59] It has been long debated whether reactive astrocytes originate from progenitor cells that migrated from the subventricular zone or whether they derive from regional mature astrocytes. Recently, several groups showed that nestin-positive subventricular zone progenitors migrate to damaged areas in the brain cortex.[60,61] Other groups demonstrated that mature astrocytes locally resume proliferation and dedifferentiate in response to brain injury and other stimuli.[57,62] Thus, both scenarios can occur. In our study, nestin-positive reactive astrocytes were observed very early during cancer cell invasion of the brain parenchyma. The origin of these astrocytes remains to be elucidated.

The reactions of microglia to cancer cells were also diverse. In the normal brain, resting or ramified microglia with thin processes are distributed throughout the brain tissue. On stimulation, ramified microglia can be progressively converted into active microglia via at least two different and functionally distinct morphological states. These are termed activated and reactive microglia.[37] Although activated microglia express only major histocompatibility complex class I, reactive microglia express both major histocompatibility complex class I and major histocompatibility complex class II and show phagocytic activity. The microglial population we found associated with cancer cells was heterogeneous and consisted of both activated microglia with typical hypertrophic stellate appearance and reactive microglia with amoeboid cell morphology. Notably, microglial responses to cancer cells were similar in immunosuppressed and in immunocompetent mice. Microglial cells can have protective as well as cytotoxic functions.[21,22] Thus, in addition to astrocytes, microglia may influence tumor cell survival and development into macrometastases.

In addition to macrometastases, we detected many solitary tumor cells distributed throughout the brain parenchyma, 30 to 70 days after carotid artery injection of MDA-MB-435 and MDA-MB-231/brain cells. The vast majority of solitary MDA-MB-435 cells were negative for Ki-67 antigen, indicating their dormant state. In contrast, solitary MDA-MB-231/brain cells and macroscopic lesions displayed similar Ki-67 expression. These observations are in line with previous reports demonstrating that cancer cells have different fates after arresting within the brain vasculature, as they may proliferate and progress to macrometastases, survive without growing (dormancy), or die and become eliminated.[63,64] In addition to the impact of clonal heterogeneity of cancer cells, local differences within the brain microenvironment, including large molecular diversity between astrocytes in different regions of the brain,[65,66] may influence the tumor cell fate. These parameters are known to affect neurogenesis and impact melanoma brain metastasis.[7,35,67] Our results demonstrate that in addition to these location-specific diversities, the invasion of brain tissue by individual cancer cells induces a variety of glial responses that add to the uniqueness of each local microenvironment. Distinct glial responses may help explain why cancer cells that arrested in the microvasculature can have different fates, even if they are located within the same brain area.[63,64] Functional contributions of different astrocytic and microglial cell populations to very early steps of metastatic invasion remain to be elucidated. Unraveling the underlying mechanisms *in vivo* might lead to targeted manipulation of the brain microenvironment for clinical inhibition of brain metastasis. Similar approaches have already been used to convert a nonneurogenic into a neurogenic environment to promote neuron formation in the adult brain.[67,68] Thus, in the future, one could envision application of these principles for treatment of brain metastasis.

Acknowledgments

We thank Hwajin Lee for his help with cutting brain cryosections, Karin Staflin for the introduction to the floating sections staining technique, Heiko Wurdak for help with confocal microscopy, and James Quigley for providing mAb 29.7.

References

1. Santarelli JG, Sarkissian V, Hou LC, Veeravagu A, Tse V: Molecular events of brain metastasis. Neurosurg Focus 2007, 22:E1
2. Al-Shamy G, Sawaya R: Management of brain metastases: the indispensable role of surgery. J Neurooncol 2009, 92:275–282
3. Albini A, Sporn MB: The tumour microenvironment as a target for chemoprevention. Nat Rev Cancer 2007, 7:139–147
4. Joyce JA, Pollard JW: Microenvironmental regulation of metastasis. Nat Rev Cancer 2009, 9:239–252
5. Witkiewicz AK, Casimiro MC, Dasgupta A, Mercier I, Wang C, Bonuccelli G, Jasmin JF, Frank PG, Pestell RG, Kleer CG, Sotgia F, Lisanti MP: Towards a new "stromal-based" classification system for human breast cancer prognosis and therapy. Cell Cycle 2009, 8:1654–1658
6. Nicolson GL, Menter DG, Herrmann JL, Yun Z, Cavanaugh P, Marchetti D: Brain metastasis: role of trophic, autocrine, and paracrine factors in tumor invasion and colonization of the central nervous system. Curr Top Microbiol Immunol 1996, 213(Pt 2):89–115
7. Zhang C, Zhang F, Tsan R, Fidler IJ: Transforming growth factor-β2 is a molecular determinant for site-specific melanoma metastasis in the brain. Cancer Res 2009, 69:828–835
8. Calabrese C, Poppleton H, Kocak M, Hogg TL, Fuller C, Hamner B, Oh EY, Gaber MW, Finklestein D, Allen M, Frank A, Bayazitov IT, Zakharenko SS, Gajjar A, Davidoff A, Gilbertson RJ: A perivascular niche for brain tumor stem cells. Cancer Cell 2007, 11:69–82
9. Carbonell WS, Ansorge O, Sibson N, Muschel R: The vascular basement membrane as "soil" in brain metastasis. PLoS One 2009, 4:e5857
10. Veeravagu A, Bababeygy SR, Kalani MY, Hou LC, Tse V: The cancer stem cell-vascular niche complex in brain tumor formation. Stem Cells Dev 2008, 17:859–867
11. Ballinger WE Jr, Schimpff RD: An experimental model for cerebral metastasis: preliminary light and ultrastructural studies. J Neuropathol Exp Neurol 1979, 38:19–34
12. Kawaguchi T, Tobai S, Nakamura K: Extravascular migration of tumor

cells in the brain: an electron microscopic study. Invasion Metastasis 1982, 2:40–50
13. Paku S, Dome B, Toth R, Timar J: Organ-specificity of the extravasation process: an ultrastructural study. Clin Exp Metastasis 2000, 18:481–492
14. Daginakatte GC, Gutmann DH: Neurofibromatosis-1 (Nf1) heterozygous brain microglia elaborate paracrine factors that promote Nf1-deficient astrocyte and glioma growth. Hum Mol Genet 2007, 16:1098–1112
15. Fitzgerald DP, Palmieri D, Hua E, Hargrave E, Herring JM, Qian Y, Vega-Valle E, Weil RJ, Stark AM, Vortmeyer AO, Steeg PS: Reactive glia are recruited by highly proliferative brain metastases of breast cancer and promote tumor cell colonization. Clin Exp Metastasis 2008, 25:799–810
16. He BP, Wang JJ, Zhang X, Wu Y, Wang M, Bay BH, Chang AY: Differential reactions of microglia to brain metastasis of lung cancer. Mol Med 2006, 12:161–170
17. Hoelzinger DB, Demuth T, Berens ME: Autocrine factors that sustain glioma invasion and paracrine biology in the brain microenvironment. J Natl Cancer Inst 2007, 99:1583–1593
18. Roggendorf W, Strupp S, Paulus W: Distribution and characterization of microglia/macrophages in human brain tumors. Acta Neuropathol 1996, 92:288–293
19. Markovic DS, Glass R, Synowitz M, Rooijen N, Kettenmann H: Microglia stimulate the invasiveness of glioma cells by increasing the activity of metalloprotease-2. J Neuropathol Exp Neurol 2005, 64:754–762
20. Markovic DS, Vinnakota K, Chirasani S, Synowitz M, Raguet H, Stock K, Sliwa M, Lehmann S, Kalin R, van Rooijen N, Holmbeck K, Heppner FL, Kiwit J, Matyash V, Lehnardt S, Kaminska B, Glass R, Kettenmann H: Gliomas induce and exploit microglial MT1-MMP expression for tumor expansion. Proc Natl Acad Sci USA 2009, 106:12530–12535
21. Murata J, Ricciardi-Castagnoli P, Dessous L'Eglise Mange P, Martin F, Juillerat-Jeanneret L: Microglial cells induce cytotoxic effects toward colon carcinoma cells: measurement of tumor cytotoxicity with a gamma-glutamyl transpeptidase assay. Int J Cancer 1997, 70:169–174
22. Zhang M, Olsson Y: Hematogenous metastases of the human brain–characteristics of peritumoral brain changes: a review. J Neurooncol 1997, 35:81–89
23. Marchetti D, Aucoin R, Blust J, Murry B, Greiter-Wilke A: p75 neurotrophin receptor functions as a survival receptor in brain-metastatic melanoma cells. J Cell Biochem 2004, 91:206–215
24. Marchetti D, Li J, Shen R: Astrocytes contribute to the brain-metastatic specificity of melanoma cells by producing heparanase. Cancer Res 2000, 60:4767–4770
25. Sierra A, Price JE, Garcia-Ramirez M, Mendez O, Lopez L, Fabra A: Astrocyte-derived cytokines contribute to the metastatic brain specificity of breast cancer cells. Lab Invest 1997, 77:357–368
26. Langley RR, Fan D, Guo L, Zhang C, Lin Q, Brantley EC, McCarty JH, Fidler IJ: Generation of an immortalized astrocyte cell line from H-2Kb-tsA58 mice to study the role of astrocytes in brain metastasis. Int J Oncol 2009, 35:665–672
27. JuanYin J, Tracy K, Zhang L, Munasinghe J, Shapiro E, Koretsky A, Kelly K: Noninvasive imaging of the functional effects of anti-VEGF therapy on tumor cell extravasation and regional blood volume in an experimental brain metastasis model. Clin Exp Metastasis 2009, 26:403–414
28. Yoneda T, Williams PJ, Hiraga T, Niewolna M, Nishimura R: A bone-seeking clone exhibits different biological properties from the MDA-MB-231 parental human breast cancer cells and a brain-seeking clone in vivo and in vitro. J Bone Miner Res 2001, 16:1486–1495
29. Lorger M, Krueger JS, O'Neal M, Staflin K, Felding-Habermann B: Activation of tumor cell integrin $\alpha_v\beta_3$ controls angiogenesis and metastatic growth in the brain. Proc Natl Acad Sci USA 2009, 106: 10666–10671
30. Deryugina EI, Quigley JP: Chick embryo chorioallantoic membrane model systems to study and visualize human tumor cell metastasis. Histochem Cell Biol 2008, 130:1119–1130
31. Lu W, Bucana CD, Schroit AJ: Pathogenesis and vascular integrity of breast cancer brain metastasis. Int J Cancer 2007, 120:1023–1026
32. Chambers AF: MDA-MB-435 and M14 cell lines: identical but not M14 melanoma? Cancer Res 2009, 69:5292–5293
33. Hollestelle A, Schutte M: Comment Re: MDA-MB-435 and M14 cell lines: identical but not M14 melanoma? Cancer Res 2009, 69:7893
34. Du R, Lu KV, Petritsch C, Liu P, Ganss R, Passegue E, Song H, Vandenberg S, Johnson RS, Werb Z, Bergers G: HIF1α induces the recruitment of bone marrow-derived vascular modulatory cells to regulate tumor angiogenesis and invasion. Cancer Cell 2008, 13:206–220
35. Fidler IJ, Schackert G, Zhang RD, Radinsky R, Fujimaki T: The biology of melanoma brain metastasis. Cancer Metastasis Rev 1999, 18:387–400
36. Puduvalli VK: Brain metastases: biology and the role of the brain microenvironment. Curr Oncol Rep 2001, 3:467–475
37. Davis EJ, Foster TD, Thomas WE: Cellular forms and functions of brain microglia. Brain Res Bull 1994, 34:73–78
38. Hayashi Y, Nomura M, Yamagishi S, Harada S, Yamashita J, Yamamoto H: Induction of various blood-brain barrier properties in non-neural endothelial cells by close apposition to co-cultured astrocytes. Glia 1997, 19:13–26
39. Hurwitz AA, Berman JW, Rashbaum WK, Lyman WD: Human fetal astrocytes induce the expression of blood-brain barrier specific proteins by autologous endothelial cells. Brain Res 1993, 625:238–243
40. Megard I, Garrigues A, Orlowski S, Jorajuria S, Clayette P, Ezan E, Mabondzo A: A co-culture-based model of human blood-brain barrier: application to active transport of indinavir and in vivo-in vitro correlation. Brain Res 2002, 927:153–167
41. Tamagno I, Schiffer D: Nestin expression in reactive astrocytes of human pathology. J Neurooncol 2006, 80:227–233
42. Hlobilkova A, Ehrmann J, Knizetova P, Krejci V, Kalita O, Kolar Z: Analysis of VEGF, Flt-1, Flk-1, nestin and MMP-9 in relation to astrocytoma pathogenesis and progression. Neoplasma 2009, 56:284–290
43. Wang HH, Hsieh HL, Wu CY, Yang CM: Oxidized low-density lipoprotein-induced matrix metalloproteinase-9 expression via PKC-δ/p42/p44 MAPK/Elk-1 cascade in brain astrocytes. Neurotox Res 2010, 17:50–65
44. Bonavia R, Bajetto A, Barbero S, Pirani P, Florio T, Schettini G: Chemokines and their receptors in the CNS: expression of CXCL12/SDF-1 and CXCR4 and their role in astrocyte proliferation. Toxicol Lett 2003, 139:181–189
45. Cui X, Chen J, Zacharek A, Li Y, Roberts C, Kapke A, Savant-Bhonsale S, Chopp M: Nitric oxide donor upregulation of stromal cell-derived factor-1/chemokine (CXC motif) receptor 4 enhances bone marrow stromal cell migration into ischemic brain after stroke. Stem Cells 2007, 25:2777–2785
46. Peng H, Erdmann N, Whitney N, Dou H, Gorantla S, Gendelman HE, Ghorpade A, Zheng J: HIV-1-infected and/or immune activated macrophages regulate astrocyte SDF-1 production through IL-1β. Glia 2006, 54:619–629
47. Xu Q, Wang S, Jiang X, Zhao Y, Gao M, Zhang Y, Wang X, Tano K, Kanehara M, Zhang W, Ishida T: Hypoxia-induced astrocytes promote the migration of neural progenitor cells via vascular endothelial factor, stem cell factor, stromal-derived factor-1α and monocyte chemoattractant protein-1 upregulation in vitro. Clin Exp Pharmacol Physiol 2007, 34:624–631
48. Nieswandt B, Hafner M, Echtenacher B, Mannel DN: Lysis of tumor cells by natural killer cells in mice is impeded by platelets. Cancer Res 1999, 59:1295–1300
49. Bos PD, Zhang XH, Nadal C, Shu W, Gomis RR, Nguyen DX, Minn AJ, van de Vijver MJ, Gerald WL, Foekens JA, Massague J: Genes that mediate breast cancer metastasis to the brain. Nature 2009, 459:1005–1009
50. Al-Mehdi AB, Tozawa K, Fisher AB, Shientag L, Lee A, Muschel RJ: Intravascular origin of metastasis from the proliferation of endothelium-attached tumor cells: a new model for metastasis. Nat Med 2000, 6:100–102
51. Chambers AF, MacDonald IC, Schmidt EE, Koop S, Morris VL, Khokha R, Groom AC: Steps in tumor metastasis: new concepts from intravital videomicroscopy. Cancer Metastasis Rev 1995, 14:279–301
52. Chambers AF, MacDonald IC, Schmidt EE, Morris VL, Groom AC: Clinical targets for anti-metastasis therapy. Adv Cancer Res 2000, 79:91–121
53. Chambers AF, Schmidt EE, MacDonald IC, Morris VL, Groom AC: Early steps in hematogenous metastasis of B16F1 melanoma cells in chick embryos studied by high-resolution intravital videomicroscopy. J Natl Cancer Inst 1992, 84:797–803
54. Kosir MA, Wang W, Zukowski KL, Tromp G, Barber J: Degradation of basement membrane by prostate tumor heparanase. J Surg Res 1999, 81:42–47
55. Kawaguchi T, Kawaguchi M, Miner KM, Lembo TM, Nicolson GL:

Brain meninges tumor formation by in vivo-selected metastatic B16 melanoma variants in mice. Clin Exp Metastasis 1983, 1:247–259
56. Bachelder RE, Crago A, Chung J, Wendt MA, Shaw LM, Robinson G, Mercurio AM: Vascular endothelial growth factor is an autocrine survival factor for neuropilin-expressing breast carcinoma cells. Cancer Res 2001, 61:5736–5740
57. Buffo A, Rite I, Tripathi P, Lepier A, Colak D, Horn AP, Mori T, Gotz M: Origin and progeny of reactive gliosis: a source of multipotent cells in the injured brain. Proc Natl Acad Sci USA 2008, 105:3581–3586
58. Itoh T, Satou T, Hashimoto S, Ito H: Isolation of neural stem cells from damaged rat cerebral cortex after traumatic brain injury. Neuroreport 2005, 16:1687–1691
59. Sofroniew MV: Reactive astrocytes in neural repair and protection. Neuroscientist 2005, 11:400–407
60. Alvarez-Buylla A, Herrera DG, Wichterle H: The subventricular zone: source of neuronal precursors for brain repair. Prog Brain Res 2000, 127:1–11
61. Faiz M, Acarin L, Villapol S, Schulz S, Castellano B, Gonzalez B: Substantial migration of SVZ cells to the cortex results in the generation of new neurons in the excitotoxically damaged immature rat brain. Mol Cell Neurosci 2008, 38:170–182
62. Ghashghaei HT, Weimer JM, Schmid RS, Yokota Y, McCarthy KD, Popko B, Anton ES: Reinduction of ErbB2 in astrocytes promotes radial glial progenitor identity in adult cerebral cortex. Genes Dev 2007, 21:3258–3271
63. Heyn C, Ronald JA, Ramadan SS, Snir JA, Barry AM, MacKenzie LT, Mikulis DJ, Palmieri D, Bronder JL, Steeg PS, Yoneda T, MacDonald IC, Chambers AF, Rutt BK, Foster PJ: In vivo MRI of cancer cell fate at the single-cell level in a mouse model of breast cancer metastasis to the brain. Magn Reson Med 2006, 56:1001–1010
64. Luzzi KJ, MacDonald IC, Schmidt EE, Kerkvliet N, Morris VL, Chambers AF, Groom AC: Multistep nature of metastatic inefficiency: dormancy of solitary cells after successful extravasation and limited survival of early micrometastases. Am J Pathol 1998, 153:865–873
65. Bachoo RM, Kim RS, Ligon KL, Maher EA, Brennan C, Billings N, Chan S, Li C, Rowitch DH, Wong WH, DePinho RA: Molecular diversity of astrocytes with implications for neurological disorders. Proc Natl Acad Sci USA 2004, 101:8384–8389
66. Wilkin GP, Marriott DR, Cholewinski AJ: Astrocyte heterogeneity. Trends Neurosci 1990, 13:43–46
67. Mori T, Buffo A, Gotz M: The novel roles of glial cells revisited: the contribution of radial glia and astrocytes to neurogenesis. Curr Top Dev Biol 2005, 69:67–99
68. Chmielnicki E, Benraiss A, Economides AN, Goldman SA: Adenovirally expressed noggin and brain-derived neurotrophic factor cooperate to induce new medium spiny neurons from resident progenitor cells in the adult striatal ventricular zone. J Neurosci 2004, 24:2133–2142

Clin Exp Metastasis
DOI 10.1007/s10585-010-9320-5

RESEARCH PAPER

Targeting activated integrin αvβ3 with patient-derived antibodies impacts late-stage multiorgan metastasis

Karin Staflin · Joseph S. Krueger · Janna Hachmann · Jane S. Forsyth · Mihaela Lorger · Sebastian C. J. Steiniger · Jenny Mee · Cristina Pop · Guy S. Salvesen · Kim D. Janda · Brunhilde Felding-Habermann

Received: 8 January 2010 / Accepted: 1 March 2010

Abstract Advanced metastatic disease is difficult to manage and specific therapeutic targets are rare. We showed earlier that metastatic breast cancer cells use the activated conformer of adhesion receptor integrin αvβ3 for dissemination. We now investigated if targeting this form of the receptor can impact advanced metastatic disease, and we analyzed the mechanisms involved. Treatment of advanced multi-organ metastasis in SCID mice with patient-derived scFv antibodies specific for activated integrin αvβ3 caused stagnation and regression of metastatic growth. The antibodies specifically localized to tumor lesions in vivo and inhibited αvβ3 ligand binding at nanomolar levels in vitro. At the cellular level, the scFs associated rapidly with high affinity αvβ3 and dissociated extremely slowly. Thus, the scFvs occupy the receptor on metastatic tumor cells for prolonged periods of time, allowing for inhibition of established cell interaction with natural αvβ3 ligands. Potential apoptosis inducing effects of the antibodies through interaction with caspase-3 were studied as potential additional mechanism of treatment response. However, in contrast to a previous concept, neither the RGD-containing ligand mimetic scFvs nor RGD peptides bound or activated caspase-3 at the cellular or molecular level. This indicates that the treatment effects seen in the animal model are primarily due to antibody interference with αvβ3 ligation. Inhibition of advanced metastatic disease by treatment with cancer patient derived single chain antibodies against the activated conformer of integrin αvβ3 identifies this form of the receptor as a suitable target for therapy.

Keywords Advanced metastasis · Treatment · Activated integrin · Patient antibodies

K. Staflin · J. S. Krueger · J. Hachmann · J. S. Forsyth · M. Lorger · B. Felding-Habermann (✉)
Department of Molecular and Experimental Medicine, The Scripps Research Institute, MEM 150, 10550 North Torrey Pines Road, La Jolla, CA 92037, USA
e-mail: brunie@scripps.edu

S. C. J. Steiniger · J. Mee · K. D. Janda
Department of Chemistry, The Scripps Research Institute, La Jolla, CA 92037, USA

C. Pop · G. S. Salvesen
Program in Cell Death and Apoptosis Research, The Burnham Institute, La Jolla, CA 92037, USA

Introduction

Advanced multi-organ metastasis is difficult to manage, and therapies could be improved if new functional targets on tumor cells were identified [1]. A potential target for inhibition of metastatic growth is the high affinity conformer of adhesion receptor integrin αvβ3. αvβ3 is an important player in tumor angiogenesis, but it also promotes tumor cell adhesion, invasive migration and survival [2–6]. The expression of αvβ3 in tumors and the tumor associated vasculature correlates with tumor grade and progression in several tumor types, most prominently in melanoma, glioma, and breast cancer [4, 7–10]. αvβ3 antagonists, including antibodies, can disrupt tumor-induced angiogenesis in animal models [11–13] and interfere with metastasis promoting tumor cell functions [14–16]. We previously documented that the activation state of αvβ3 is critical for supporting metastatic progression and that the high affinity form of αvβ3 identifies a metastatic subset of tumor cells [5]. Interestingly, we also found that the immune repertoire of cancer patients can contain anti-tumor antibodies, which specifically react with

Published online: 12 March 2010

the activated form of αvβ3. These antibodies are ligand-mimetics of the αvβ3 integrin and carry an Arg-Gly-Asp (RGD) sequence within their CDR-H3 regions [17].

In the present study, we investigated whether targeting the high affinity conformer of integrin αvβ3 with the ligand mimetic antibodies can interfere with advanced metastatic disease. This was examined in immune deficient mice after inducing progressive metastatic burden with human tumor cells expressing high affinity αvβ3. Response to treatment was followed with non-invasive bioluminescence imaging. The observed anti-metastatic properties of the scFv antibodies are due to their ability to specifically and nearly irreversibly bind and inhibit the activated conformer of αvβ3. Thus, activated αvβ3 appears as a suitable target for the inhibition of widespread metastatic disease. The fully human antibodies used in this study and their derivatives, or compounds with similar specific properties, might provide a basis for powerful therapeutic intervention of advanced metastasis.

Results

The main goal of this study was to investigate if the high affinity conformer of tumor cell integrin αvβ3 is a suitable target for inhibition of advanced and widespread metastatic disease. We used human tumor cell models expressing activated αvβ3 in immune deficient mice, and analyzed the ability of patient derived scFv antibodies against this form of the receptor to interfere with advanced metastatic progression.

Antibody binding validation and routes of administration

To test in principle whether targeting activated αvβ3 with the ligand mimetic scFvs interfere with advanced metastatic disease, we chose a phage-displayed format of the antibodies for treatment. By using this format, we took advantage of the tissue penetrating properties of phage and their ability for multivalent antibody display [18]. To verify the cell binding characteristics of the phage antibodies, we analyzed each scFv-phage batch for tumor cell binding before using the material for animal treatment. ScFv phage binding was examined on two different tumor cell models, each expressing the activated form of integrin αvβ3, namely M21 human melanoma cells (high αvβ3 expression) and MDA-MB-435 $\beta3_{D723R}$ human metastatic cancer cells [5] (intermediate αvβ3 expression). Binding of αvβ3 directed scFv1- and scFv5-phage was compared to wild type phage as a control (Fig. 1a). Appropriate routes of administration and in vivo distribution of scFv phage were examined in non-tumor bearing mice to assess if and to what extent the antibodies were able to reach major target organs of metastasis, without the bias of tumor burden there. Inoculation of 5×10^{10} scFv1 or scFv5 phage intranasally, intravenously or intraperitoneally lead to efficient phage recovery from the lungs, brain, liver, and kidneys of SCID mice 24 h after scFv injection (Fig. 1b shows scFv5). Intravenous and intraperitoneal routes produced the highest phage titers in the examined organs ($>1 \times 10^8$ phages per gram of tissue). The lowest titer was found in the brain. Having established that scFv phage can

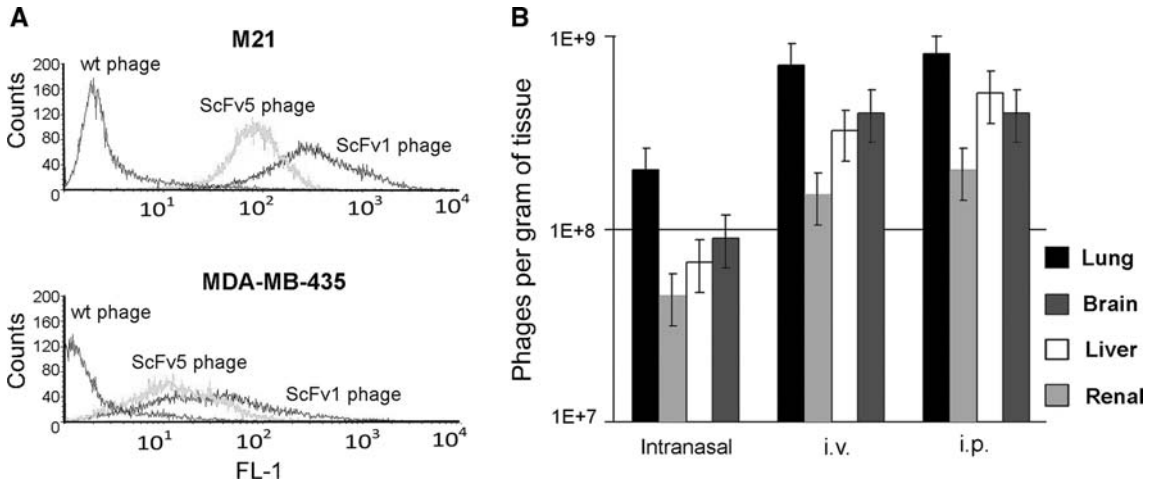

Fig. 1 Antibody binding validation and routes of administration. **a** Before use in animals, the binding properties of each scFv phage batch were analyzed by flow cytometry on tumor cells expressing high affinity integrin αvβ3. scFv phage was tested in the presence of calcium on M21 human melanoma cells that carry activated αvβ3 and on MDA-MB 435 cells which express mutant $\alpha v\beta3_{D723R}$. **b** scFv phage organ distribution in the mouse model. Phage were injected i.v., i.p. or applied intranasally to non-tumor bearing mice to determine phage organ distribution 24 h later

reach sites that are most frequently involved in metastasis, we chose the intraperitoneal route for scFv phage treatment of tumor bearing animals, as this route lead to high phage tissue recovery and can be used repeatedly for treatment.

Treatment of metastatic disease with scFv antibodies targeting activated integrin $\alpha v\beta 3$

Metastasis was induced in SCID mice by injecting MDA-MB-435 human metastatic cancer cells [19, 20] into the venous circulation. The tumor cells were stably tagged with firefly luciferase to follow their growth and response to treatment based on non-invasive longitudinal measurements by bioluminescence signal of whole body imaging. For the treatment studies, scFv phage purification was optimized to remove endotoxin, and it was verified that phage injection had no adverse side effects. Metastatic burden was monitored in each animal over time and measured based on photon flux (p/s/cm^2). The fold-change in lesion growth under treatment was calculated by comparing lesion growth during a given number of days before treatment and the same number of days under treatment.

An overview of treatment responsiveness in animals with advanced metastatic burden and response types is given in Table 1. The results indicate that scFv1 or scFv5 treatment interfered with in vivo growth of metastatic lesions in a significant number of animals compared to treatment controls ($P = 0.0164$ by Fisher exact test).

Table 1 Overview of treatment responsiveness in animals with advanced metastatic burden and response types

Response category	ScFv1	ScFv5	Control
Progression	7/19	9/15	15/16
Stabilization	4/19	1/15	1/16
Reduced progression	4/19	3/15	0/16
Regression	4/19	2/15	0/16

Response categories: fold-changes in overall lesion growth, p/sec/cm^2, comparing same time span before and under treatment

Progression: $\geq$1.3-fold

Stabilization: 0.7–1.3-fold

Reduced progression: 0.1–0.7-fold

Regression: $\leq$0.1-fold

Compared to controls, treatment response was seen in a significant number of animals receiving scFv1 or scFv5 ($P = 0.0164$, Fisher exact test). There was no significant difference between responses to scFv1 compared to scFv5 ($P = 0.55$, Fisher's exact test)

For comparison of responses between the three groups, scFv1, scFv5, and controls, we note that the overall likelihood ratio chi-squared statistic with six degrees of freedom may be partitioned into two independent components, each with three degrees of freedom: the first component corresponds to comparison of scFv1 vs scFv5, and the second component corresponds to the comparison of controls to the pooled scFv1/scFv5 category [45]

Treatment response measurements initially focused on lung lesions because these represented the strongest burden and were consistently found. Figure 2 shows mice where metastatic lesions were allowed to develop for 56 days before starting i.p. treatment with scFv1 or scFv 5 phage (5×10^{10}). The animals in panels A–C had received 1×10^5 tumor cells and were treated every 48 h for 7 days (four doses). The percentage of responding animals was 57% in the scFv1 group, and 60% in the scFv5 group. To challenge the therapeutic approach and assess treatment responses in mice with even stronger metastatic burden, mice as shown in panel D were injected with 2.5×10^5 tumor cells and received treatment on day 56 given every 24 h (eight doses). Under these conditions, the response rate was 75% in the scFv1 group, and 25% in the scFv5 group. All control animals showed continuous lesion progression. Treatment efficacy of scFv1 was higher than that of scFv5. This finding corresponds to an enhanced potency of scFv1 for interfering with $\alpha v\beta 3$ integrin ligand binding, as shown below. The results indicate that targeting the high affinity form of integrin $\alpha v\beta 3$ can impact advanced metastatic burden and slow its growth.

To emulate a clinical situation where patients may present with widespread advanced metastatic disease to multiple organs, and to monitor treatment response of lesions at individual target sites, we injected SCID mice i.v. with a subline of MDA-MD 435 (MDA-MB 435 met) that we selected in vivo. This subline expresses intrinsically activated integrin $\alpha v\beta 3$, and consistently causes multiorgan metastasis. All injected mice developed metastatic lesions in multiple target organs, including the brain, lymph nodes, liver, spleen, bone, kidneys and lungs. We selected the animals with the highest tumor burden and the most widespread metastasis for therapy with scFv1 or scFv 5 phage. Individual animals had metastases in up to three different organs. In all cases, these included the lung. The animals were treated every 24 h for 7 days with 5×10^{10} scFv1 or scFv5 phage, and lesion growth was monitored by bioluminescence imaging. The results are summarized in Table 2, reporting regression of pulmonary and extrapulmonary metastases in the treatment groups. Examples of regression in renal metastases in response to only three doses of scFv1 treatment are shown in Fig. 3. In one case, an adrenal lesion, clearly documented before treatment, disappeared and was no longer detectable by non-invasive whole body imaging (Fig. 3a Mouse 1) or by ex vivo imaging of the excised organ. In another case, a large adrenal lesion clearly regressed in response to scFv1 (Fig. 3a Mouse 2).

Metastatic lesions in different organs within the same animal sometimes showed distinct responses to treatment. There was no apparent correlation between lesion size at the beginning of treatment and the ability to respond.

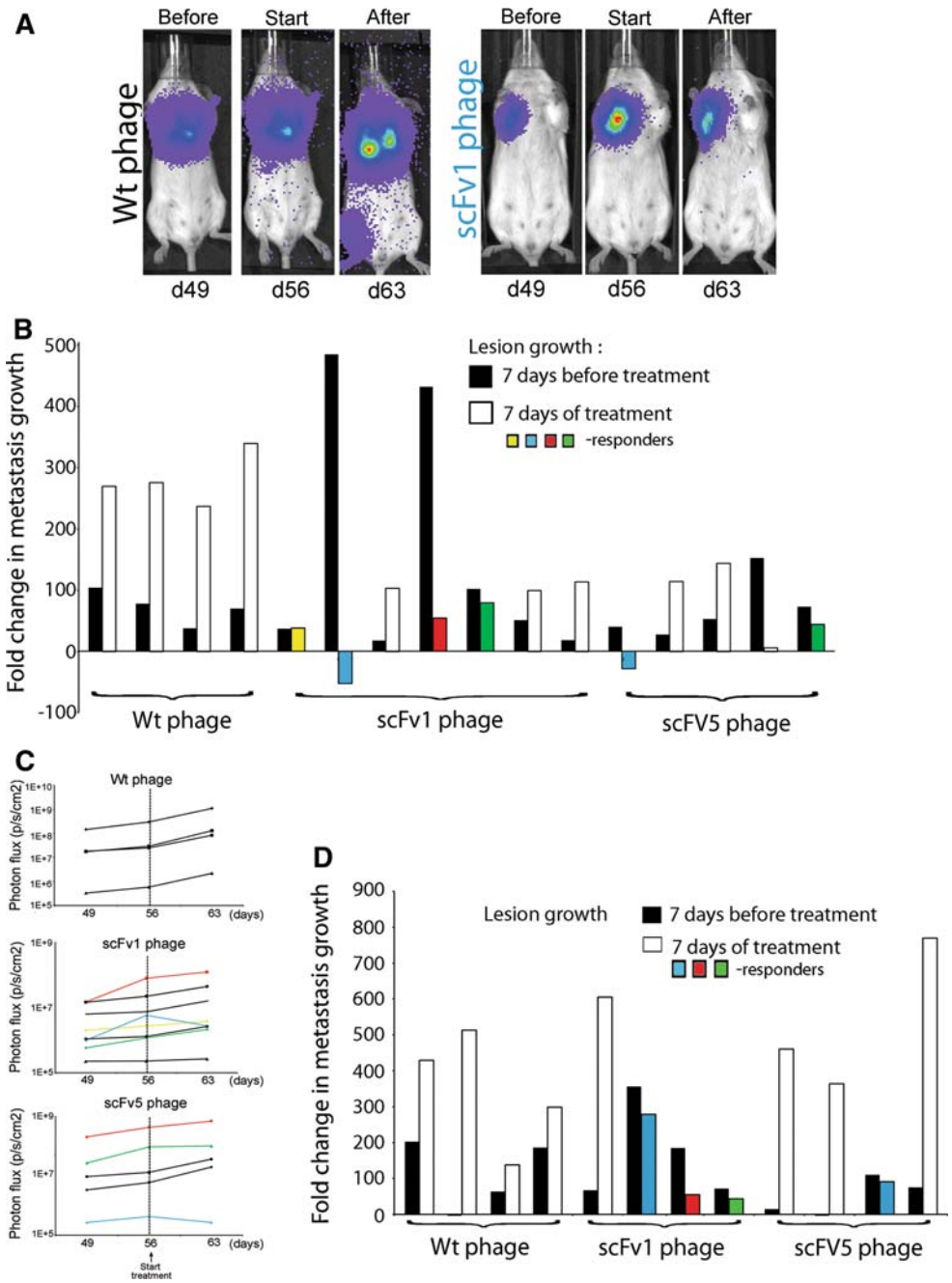

Fig. 2 Lung metastases regress in response to treatment with scFv 1 or scFv 5. *F-luc* tagged MDA-MB-435 cells were injected i.v. and lesion development monitored by non-invasive bioluminescence imaging (photons/second/cm^2) over time. Treatment with scFv phage (5×10^{10} per dose) started on day 56 post tumor cell injection. **a** Examples of non- invasive bioluminescence imaging of representative animals that had received 1×10^5 tumor cells before treatment on day 49, at treatment onset on day 56, and after four doses of treatment on day 63. Reduced progression in lung lesions is seen after treatment with scFv1 but not with Wt-phage. **b** Response to treatment given every 48 h (four doses). Fold-changes of lesion growth were calculated based on growth during 7 days before treatment compared to 7 days under treatment. ScFv1-phage treatment yielded a 57% animal response rate in lung burden and one animal with stabilization of lesion growth. ScFv5-phage treatment resulted in a 60% animal response rate for lung burden. Wt-phage gave no reduction in tumor growth. **c** *Non*-invasive bioluminescence imaging of lung burden (photons/second/cm^2) over time before and during treatment. Animals were treated every 48 h for (four doses). Lung lesion growth was monitored pre-treatment (day 49–56) and during treatment until day 63 (the end of treatment). *Dashed vertical lines* indicate the start of treatment on day 56. Animals responding to treatment are colored. **d** Response of mice with very advanced metastatic burden, induced by injecting 2.5×10^5 tumor cells, to treatment given every 24 h (eight doses). Treatment with Wt-phage gave no response, whereas regression and reduced tumor progression was seen in the scFv treated animals. ScFv1-phage treatment yielded a response in 75% of the animals, and scFv5-phage in 25%. Animals responding to treatment are colored

Table 2 Overview of regresssion in multiorgan metastasis

Regression	ScFv 1	ScFv 5	Control
Pulmonary lesions	3/9	2/6	0/7
Extrapulmonary lesions	4/9	0/6	0/7

Regression of metastatic burden was based on comparing lesion growth during the same time before versus under treatment, measured by bioluminescence imaging and fold-changes in photon flux (p/sec/cm^2) as in Table 1. Due to the heterogeneity of lesion burden and organ involvement, only regression responses are shown, and pulmonary versus extrapulmonary lesions are listed separately. Considering responses of lesions at all sites, scFv1—but not scFv5—lead to regression of multi-organ metastasis in a significant number of animals (7/9 scFv1, 2/6 scFv5, 0/7 control; $P = 0.0073$ Fisher's exact test)

Differences in the vascularity of the lesions and vascular functionality, as well as heterogeneity of individual lesions might contribute to this observation. Overall, scFv1 treatment induced regression in multi-organ metastasis more efficiently than scFv5. All animals treated with control phage showed continuous progression in individual lesions and overall tumor burden.

In vivo localization of scFv to metastatic lesions and in situ treatment response

Having evidence that scFv1 or scFv 5 treatment directed against the high affinity conformer of integrin $\alpha v\beta 3$ can interfere with advanced metastatic growth, we investigated whether the antibodies actually reached the tumor cells within metastatic lesions to assess whether the tumor cells are direct targets of this treatment. To track the antibodies in lesion bearing animals that had received scFv1 or scFv5, the animals were terminally perfused 24 h after the last antibody dose and cryosections prepared of control and tumor bearing organs. Tumor cells were identified by staining for human CD44 [21] (dark blue in Fig. 4a), and scFv phage was detected with anti-M13 (brown in Fig. 4a or red fluorescence in b). As indicated in Fig. 4a, showing phage signal within metastatic lesion tissue particularly at higher magnification (right panel), and clearly seen by imunofluorescence staining in Fig. 4b, ScFv1 and scFv 5 phage specifically accumulated within metastatic lesions and in their immediate proximity. This was observed in different organs with metastatic burden, but not in non-tumor bearing tissues. Wild type phage, used as a control, did not accumulate at tumor lesions. Non-tumor bearing tissues sporadically showed a faint signal for wild type phage, but not associated with any specific cell type. Figure 4 documents that scFv1 and scFv5 phage localized to lung or lymph node metastases. In some cases, scFv signal was found directly associated with the tumor cells. An example of a lung lesion is shown by deconvolution microscopy in Fig. 4b (bottom row). These results indicate that the ligand mimetic antibodies, directed against the activated conformer of integrin $\alpha v\beta 3$, localized to advanced metastatic lesions in the mouse model in a therapeutic setting. Integrin $\alpha v\beta 3$ is known to be a key player in angiogenesis, and the activated form of the receptor is expressed by sprouting endothelial cells [22]. We found that the patient derived antibodies, scFv1 and scFv5, react with the murine antigen (by flow cytometry on proliferating murine endothelial cells and the Bend3 endothelial cell line, not shown). However, there was no difference in micro vessel density within lung tumor lesions in control versus antibody treated animals. This was

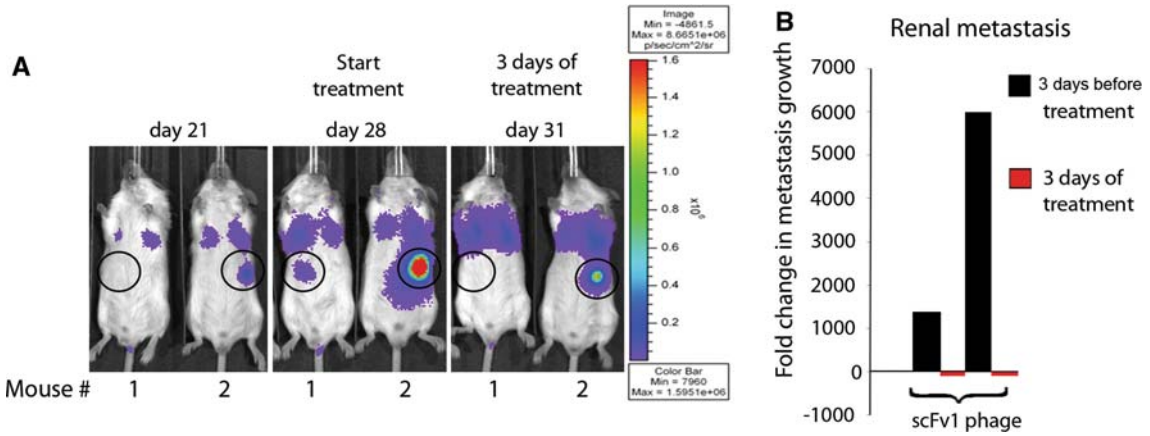

Fig. 3 Examples of extrapulmonary lesion regression under treatment with scFv 1. **a** *F-luc* tagged, in vivo selected and highly metastatic MDA-MB-435-met cells were injected i.v. to induce multiorgan metastasis. Metastatic progression was monitored by non-invasive bioluminescence imaging (photons/second/cm^2) over time. In these examples, the location of renal lesions is circled and shown 3 days before treatment, at the beginning of treatment, and after three daily doses of scFv1 phage. **b** Fold-change in renal lesion growth, calculated based on signal change during 3 days before and 3 days under treatment

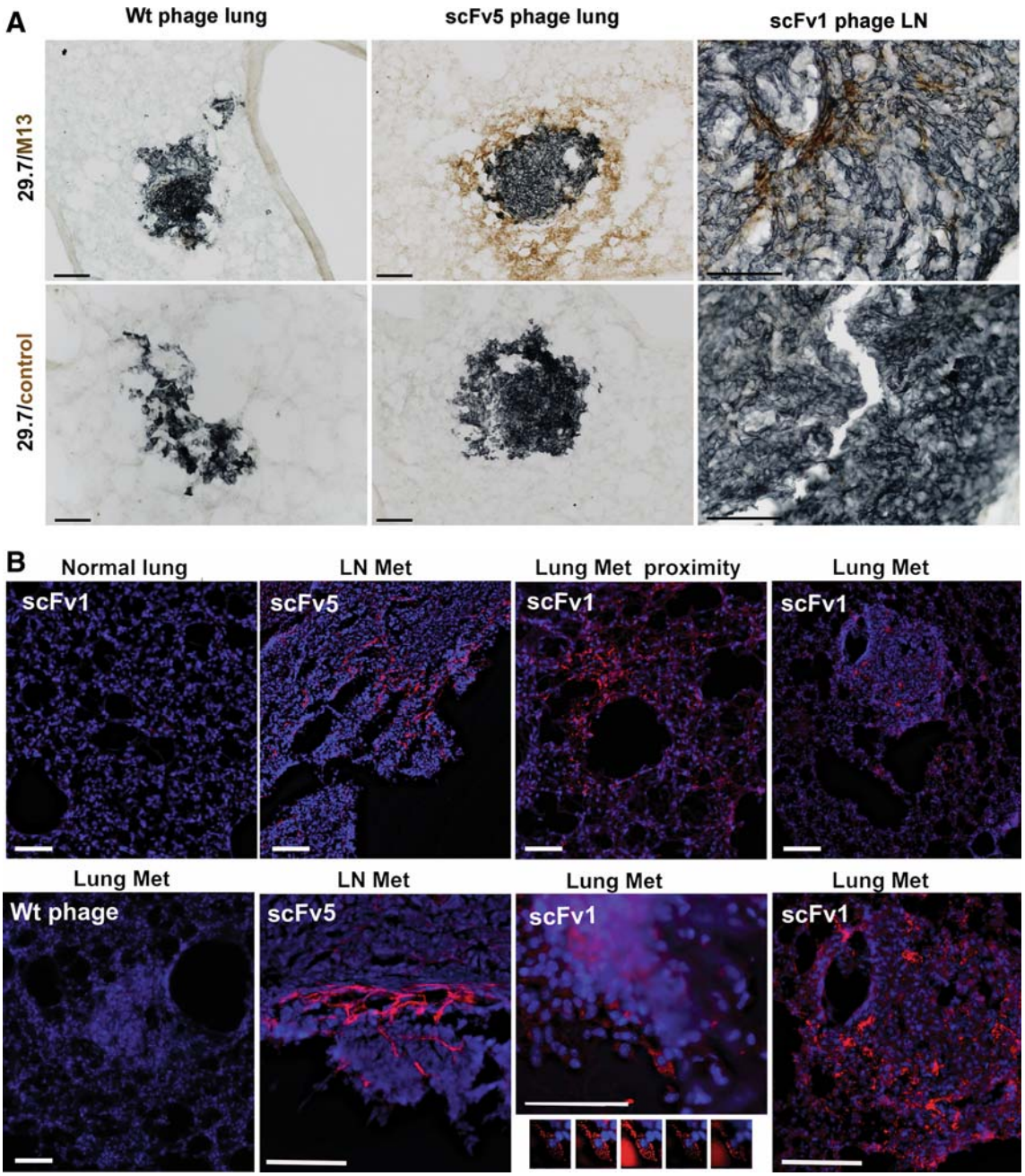

Fig. 4 Localization of scFv1 or scFv 5 phage to areas in and around metastatic lesions in mice with multi-organ metastasis. **a** Immunohistochemical detection of phage homing to metastases in the lungs and lymph node. ScFv phage, or wt control phage, were injected i.p. daily for 7 days into tumor bearing mice. 24 h after the last scFv dose, the animals were terminally perfused and frozen tissue sections stained with mAb 29.7 (*dark blue*), specific for human CD44 indicating the tumor cells, and anti-M13 mAb to detect phage (*DAB*, *brown*). Animals treated with wt-phage did not show phage localization to tumor metastases (*left panels*), but lung metastasis from scFv5-phage treated animals showed phage localization in the tumor proximity as well as within the lung lesion (*middle*). A lymph node metastasis from an animal treated with scFv1-phage showed phage localizing to the tumor bulk as well as to the outer border of the lesion (*right*). Controls treated with secondary antibody and substrate did not show specific staining in or around any lesions. *Scale bars* indicate 100 μm. **b** Fluorescence microscopy detecting phage (*red*). (*Upper row*) M13 phage was detected in and around lung metastases of scFv1-phage treated animals (*right*), as well as within the near proximity of the tumor lesions (*second right*), with minimal phage signal in the unaffected lung tissue away from a tumor lesion (*left*). Lymph node metastasis showed scFv1-phage localization in the tumor mass and within the tumor proximity (*second left, top and bottom*). Animals treated with wt-phage showed no specific staining in tumor lesions. Only a weak signal was sometimes seen in non-tumor bearing parts of the tissues, comparable to that seen for scFv phage in unaffected areas of lung tissue (*lower left*). Using optical sectioning and deconvolution of *z*-stack images, scFv phage was specifically detected associated with tumor cells (*lower second right*). *Scale bars* indicate 100 μm

measured on anti- CD34 stained step sections covering 600–800 μm depth of lung tissue (data not shown). There was a tendency for fewer lesions in the lungs of animals responding to treatment (1–9 lesions) compared to controls (10–25 lesions).

To investigate how scFv treatment targeting the activated conformer of integrin $\alpha v\beta 3$ affects lesion development in vivo, we studied cell cycle marker expression in lung metastases that responded to scFv treatment. Compared to controls, the number of proliferating Ki67-positive cells was significantly reduced in lesions responding to treatment (Fig. 5a). Expressed as percent area covered by Ki67 signal of total lesion area measured, the mean Ki67 reactivity in control and non-responding lesions was 38.1 ± 6.9, and $19.9 \pm 7.4\%$ in responding lesions ($P = 0.0159$). In addition, the responding lesions showed enhanced infiltration by activated macrophages (F4/80 signal; Fig. 5b). The results indicate that scFv treatment affected the growth rate of metastatic lesions at the cellular level and involved host cell responses. These responses potentially helped to clear apoptotic or dead tumor cells, which were rarely detected (not shown).

Inhibition of receptor-ligand binding at the molecular level

To investigate mechanisms involved in the observed treatment responses, we studied the interactions of the ligand-mimetic antibodies and integrin $\alpha v\beta 3$ at the molecular and cellular levels.

To assess molecular interactions between integrin $\alpha v\beta 3$ and the scFv antibodies, we analyzed their ability to interfere with ligand binding to the purified receptor. Vitronectin, fibronectin and fibrinogen are natural ligands of $\alpha v\beta 3$ in extracellular matrices and plasma. A hallmark characteristic of the activated conformer of $\alpha v\beta 3$ is that the receptor can recognize these ligands as soluble proteins. Incubation of the biotinylated proteins with immobilized $\alpha v\beta 3$ in the presence of cations and increasing concentrations of the antibodies showed that scFv 1 and scFv 5 efficiently interfered with

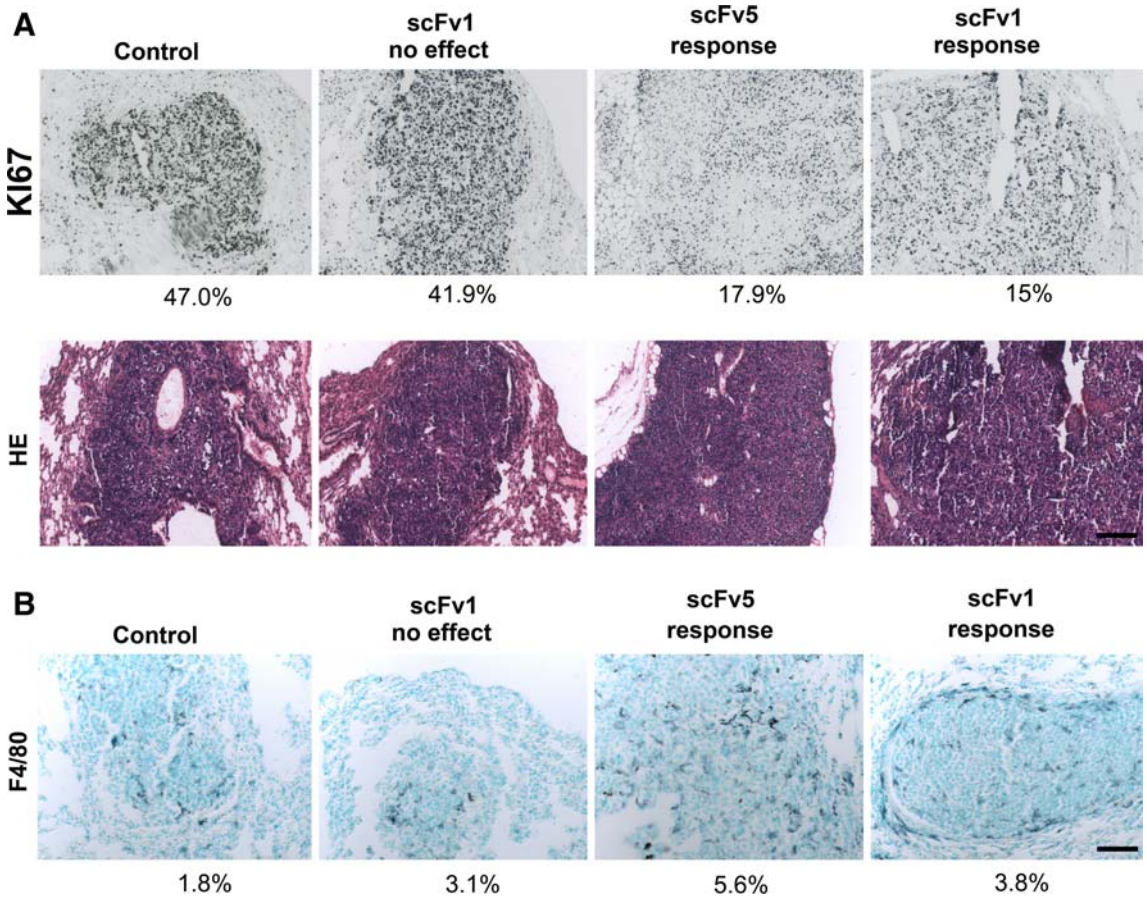

Fig. 5 Effects of scFv treatment on tumor cells in vivo and host cell infiltration **a** Ki67 staining of lung metastases treated with wt-phage or scFv1/5-phage (*top panel*). Lesions in animals responding to treatment showed fewer proliferating cells. Percent area covered by Ki67 signal relative to lesion area measured. H&E staining of the lesions (*lower panel*). **b** F4/80 macrophage staining of lung metastases in mice treated with wt-phage or scFv1/5-phage. An increased infiltrate was seen in lesions responding to treatment. Percent area covered by F4/80 signal relative to lesion area measured. *Scale bars* indicate 100 μm in all sections

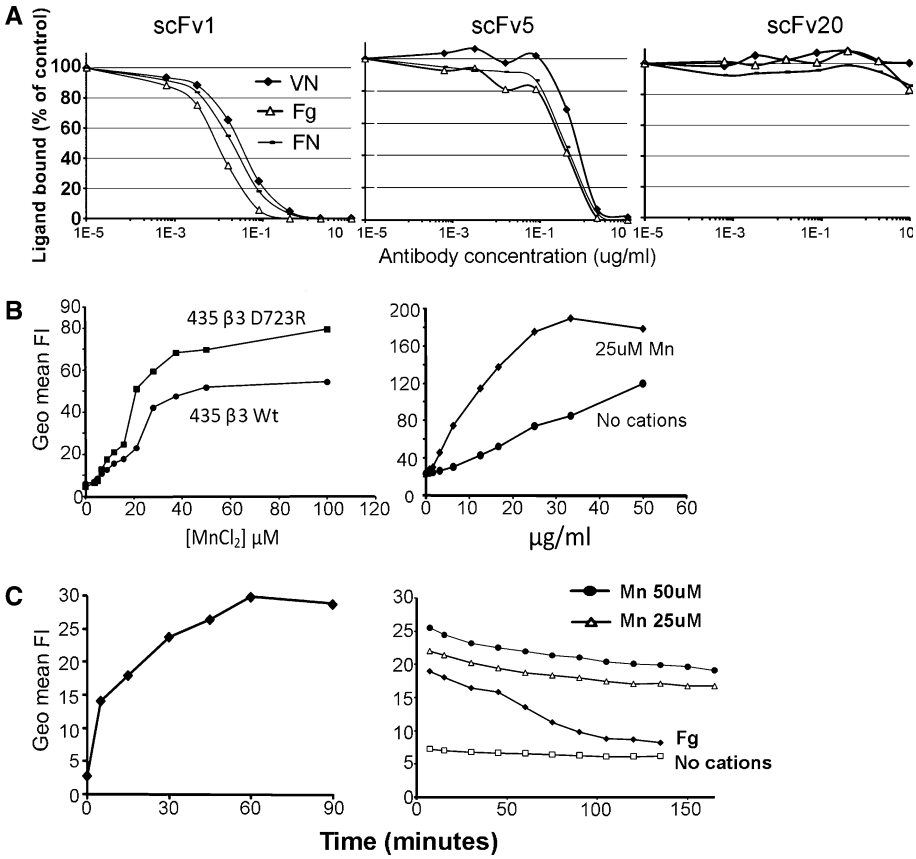

Fig. 6 Inhibitory and binding properties of scFv 1 and scFv5. **a** Biotinylated natural ligands of $\alpha v\beta 3$: vitronectin (*VN*), fibronectin (*FN*) or fibrinogen (*Fg*; 10 μg/ml) were incubated with purified immobilized $\alpha v\beta 3$ receptor protein in TBS containing Ca^{2+}, Mg^{2+}, and Mn^{2+} (1 mM each), in the presence of increasing concentrations of purified scFv protein. A non-function blocking scFv directed against the integrin αv subunit, scFv 20, was used as a control. **b** Flow cytometric binding analysis of fluorescinated scFv5 protein and MDA-MB 435 human tumor cells, expressing either activated high-affinity $\alpha v\beta 3_{D723R}$ or non-activated $\alpha v\beta 3_{WT}$. Binding was experimentally maximized in the presence of Mn^{2+}, known to induce a high affinity state in integrin heterodimers. Using a Mn^{2+} concentration (25 μM) that supports suboptimal scFv5 binding to tumor cells expressing activated $\alpha v\beta 3_{D723R}$, antibody was titrated to determine binding saturation. **c** Kinetics of scFv cell association and dissociation were analyzed by flow cytometry with FITC-labeled scFv protein at half maximal Mn^{2+} concentration and saturating scFv concentration, using MDA-MB-$435_{\beta 3D723R}$ cells. (*Left*) Association time was measured after removing unbound ligand in 10 min intervals. (*Right*) Dissociation was determined after allowing cells to bind scFv for 1 h to reach binding saturation, followed by removal of unbound ligand, washing and measuring scFv that remained bound in 10 min intervals. FITC-labeled Fg was used as a natural ligand for comparison. All incubations were done on ice using ice-cold buffers to prevent scFv or ligand internalization. No binding was detected in the absence of divalent cations

$\alpha v\beta 3$ ligand binding (Fig. 6a). The half maximal inhibitory concentrations (IC_{50}) for scFv 1 were 1.25 nM for vitronectin, 0.71 nM for fibronectin, and 0.35 nM for fibrinogen. For scFv 5, the IC_{50} values were 25 nM for vitronectin, 12.5 nM for fibronectin, and 10.7 nM for fibrinogen. ScFv20 used as a control antibody failed to inhibit. While patient derived scFv antibodies scFv 1 and scFv 5 contain the RGD integrin binding motif within their CDR-H3 regions and are specific for $\alpha v\beta 3$, scFv 20 lacks the RGD motif, does not block function and detects αv integrins regardless of their β subunit association [17]. The results demonstrate that scFv1 and scFv 5 have a high affinity for $\alpha v\beta 3$ and compete very effectively with ligands binding to this receptor. The increased inhibitory efficacy of scFv1 over scFv5 at the molecular level is reflected in the increased anti-cancer efficacy of scFv1 seen in vivo.

Characteristics of scFv binding to human tumor cells expressing activated integrin $\alpha v\beta 3$

To understand inhibitory activities of scFv1 and scFv5 on tumor cell functions that rely on integrin $\alpha v\beta 3$ and might promote metastasis, we analyzed interaction between the scFvs and tumor cell expressed $\alpha v\beta 3$. Integrin binding of natural ligands in their soluble form requires the high affinity state of the receptor [23]. Furthermore, tumor cells within target tissues interact dynamically with components of the extracellular matrix and derive signals from their

matrix environment for survival and growth. To investigate the binding characteristics of tumor cell expressed high affinity $\alpha v\beta 3$ and the ligand mimetic scFvs, we analyzed cellular association and dissociation. All scFv cell binding experiments were carried out at 0°C to prevent internalization. Flow cytometry binding analysis of fluorescinated scFv5 protein and MDA-MB 435 human metastatic cancer cells, expressing either activated high-affinity $\alpha v\beta 3_{D723R}$ or non-activated $\alpha v\beta 3_{WT}$, indicated that the ligand-mimetic antibody depended on $\alpha v\beta 3$ activation for efficient binding. Binding was experimentally maximized in the presence of Mn^{2+} (Fig. 6b, left panel), a cation known to induce a high affinity state in integrin heterodimers [24–26]. Using a Mn^{2+} concentration (25 μM) that supports suboptimal (75%) scFv5 binding to tumor cells expressing the intrinsically activated receptor ($\beta 3_{D723R}$ mutant), we titrated the antibody to determine binding saturation. Saturable binding in the presence of divalent cations indicated specificity and cation dependence (Fig. 6b, right panel). These findings underscore the ligand mimetic nature of the scFv antibodies and define conditions suitable to determine cellular association and dissociation of the antibodies. The association and dissociation characteristics are important for understanding the therapeutic potential of the antibodies and their ability to interfere with established $\alpha v\beta 3$ ligand interactions. Such interactions support tumor cell integration and growth within target tissues of metastasis.

Using tumor cells expressing intrinsically activated $\alpha v\beta 3_{D723R}$ and 25μM Mn^{2+}, we found that the ligand mimetic antibodies scFv1 and scFv5 exhibit a fast cellular association rate, with half maximal binding observed after 5 min, the earliest measured time point (shown for scFv 5 in Fig. 6c, left panel). In contrast, scFv dissociation after binding saturation was exceedingly slow, with only 22% binding loss after 160 min, whereas binding of fibrinogen, a natural ligand of $\alpha v\beta 3$, was reduced by 50% after 60 min, and 88% after 120 min (Fig. 6c, right panel). These results indicate that the ligand mimetic antibodies can occupy the receptor efficiently and stay bound for prolonged periods of time. Thereby the antibodies may displace natural ligands that dissociate off the receptor. Based on these properties, the antibodies efficiently interfere with dynamic $\alpha v\beta 3$ mediated cell adhesive functions during cell migration and invasion as previously seen in vitro [17]. Importantly, the observed scFv cell binding characteristics likely enable the antibodies to interfere with tumor cell behavior in vivo and to disrupt established tumor cell adhesion mediated by integrin $\alpha v\beta 3$.

Analysis of caspase-3 activation by the RGD-containing scFv antibodies

The in vivo responses to treatment with the $\alpha v\beta 3$ ligand-mimetic scFv antibodies may have diverse underlying reasons. The antibodies could exert their therapeutic effects primarily through their ligand-mimetic nature interfering with $\alpha v\beta 3$ ligand binding. However, additional mechanisms may also be involved. We previously showed that scFv 1 and scFv 5 are internalized by tumor cells expressing activated integrin $\alpha v\beta 3$ and induce apoptosis [17]. We therefore reasoned that the internalized RGD-containing scFvs might interact with intracellular proteins, such as the apoptosis inducing caspase-3. Caspase-3 contains a putative RGD binding site, close to its Asp^{175} cleavage site (Asp-Asp-Met, DDM) [27, 28]. A previously reported intriguing concept suggested that cell internalized RGD peptides might induce apoptosis by directly binding and activating caspase-3 [27, 29, 30]. To explore if such a mechanism might be involved in the observed anti-metastatic properties of the RGD containing scFv antibodies, we verified that the tumor cells used in our treatment study expressed caspase-3, and analyzed if the scFvs could directly interact with caspase-3 and activate the enzyme.

We confirmed caspase-3 expression in MDA-MB-435 human tumor cells used in our in vivo treatment study (Fig. 7a). MCF7 cells lacking caspase-3 [31] were used as negative control, and SKBr3 [32] as positive control. To investigate if RGD containing scFv 1 and scFv 5 can directly bind caspase-3, we analyzed whether the scFvs immuno-precipitate caspase-3 from tumor cell lysates, or if the scFvs—added to tumor cell lysates—could be co-immunoprecipitated with anti-caspase-3. We found no evidence of scFvs caspase-3 interaction (not shown). Furthermore, we found no interaction between recombinant caspase-3 and RGD-containing scFv1 or scFv5 by ELISA under various cation conditions known to affect RGD binding (Fig. 7b).

Once internalized by cells, RGD-containing proteins might transiently interact with caspase-3 in a biologically relevant but difficult to detect manner. Considering the therapeutic effects on metastatic growth by the RGD-containing scFvs in our animal model, we therefore investigated whether the scFvs could contribute to caspase-3 activation in cell lysates and by using recombinant human caspase-3 protein. Hypotonic lysates of 293A cells, deprived of mitochondria and containing caspase-3, were readily activated by addition of cytochrome *c* and dATP to form apoptosomes that can activate caspase-3 (Fig. 7c, d). Cofactors in these gently generated lysates promote the stability of procaspase-3 and support its activation. In contrast, RGD-containing scFv 5, or RGD peptides, showed no induction of caspase-3 activity over RGE-containing scFv Mut5, or RAD, as negative controls. Similar results were obtained despite increasing scFv concentrations, and after investigating the kinetics of caspase-3 activation by continuous measurement of substrate cleavage over time (Fig. 7d). Likewise, reducing the complexity

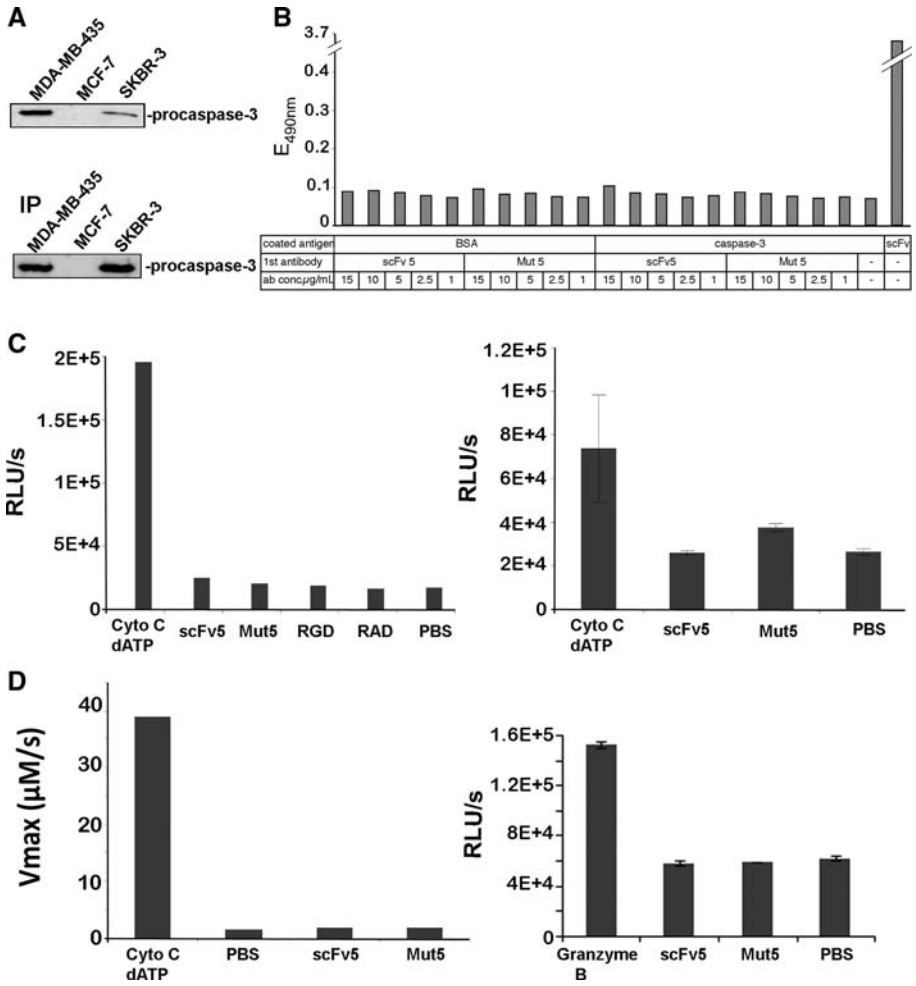

Fig. 7 Caspase-3 expression in the target tumor cells and analysis of caspase-3 binding and activation by RGD-containing scFv1 and scFv5. **a** (*Top*) Western blot analysis of caspase-3 expression in MDA-MB-435, MCF-7 (negative control) and SKBR-3 (positive control) cells. (*Bottom*) Verification for procaspase-3 by immunoprecipitation of caspase-3 from tumor cell lysates. **b** ELISA-based analysis of caspase-3 and scFv antibody interaction. Plates were coated with recombinant pro-caspase-3 or BSA (negative control) or scFv 5 (positive control). Addition of RGD-containing scFv 5 or RGE-containing scFv Mut 5 antibody, at concentrations as indicated showed no specific binding to caspase-3. **c** Analysis of caspase-3 activation by scFv antibodies. Hypotonic cell lysates, depleted of mitochondria, were combined with either scFv 5 or scFvMut 5 (4 µM), or RGD or RAD peptides (1 mM) (left panel). Cytochrome *c*/dATP were used as positive control and PBS as negative control in a bioluminescence assay. Cytochrome *c* and dATP were able to activate caspase-3 in the lysates, whereas all other samples showed only background signal. A higher scFv concentration was used to verify the lack of activation (10 µM) in the presence of Mg^{2+} (right panel). **d** Continuous measurement of caspase-3 activity in cell lysates based on chromogenic substrate reaction. Cleavage of colorimetric capsase 3 substrate N-acetyl-Asp-Glu-Val-Asp-*p*-nitroanilide (Ac-DEVD-*p*NA) was measured after combining hypotonic cell lysates with either scFv 5 or scFvMut 5 (2 µM). Absorption was measured continuously for 2 h at 37°C (*left panel*). Activation measurement of recombinant caspase-3 by scFv 5 or scFvMut 5 in the presence of Mg^{2+} using Granzyme B as positive and PBS as negative control. After 30 min incubation at 37°C, Glo reagent was added and bioluminescence measured after 30 min incubation at RT (*right panel*)

of the assay system further and using recombinant caspase-3 to ensure that the reaction and potential interaction between caspase-3 and scFv antibody was not influenced by components present in cells or cell lysates, did not reveal RGD induced caspase-3 activation (Fig. 7d, right). Thus, these results make it very unlikely that the internalized RGD-containing antibodies scFv1 or scFv5 induce apoptosis by direct activation of caspase-3. We therefore conclude that the inhibitory properties and in vivo treatment effects, that the antibodies exerted on tumor cells expressing the activated conformer of integrin $\alpha v\beta 3$ and their metastatic lesions, are most likely based on the ability of the antibodies to interfere efficiently with ligand binding to the target integrin.

Discussion

Metastatic disease is mainly treated with chemotherapy to halt tumor growth or with specific inhibitors of receptors

and pathways to interfere with tumor cell viability. Development of effective combinations of such therapies and discovery of new targets are urgently needed to improve therapeutic responses.

Our study explored the high affinity, activated conformer of integrin $\alpha v\beta 3$ on metastatic tumor cells as a functional target for therapy with human antibodies that specifically recognize and block this form of the receptor. We showed earlier that a metastatic subset of human tumor cells expresses the activated integrin and uses this form of the receptor for successful early steps of dissemination to distant organs [5]. Interestingly, the immune repertoire of cancer patients contains antibodies that recognize the high affinity form of $\alpha v\beta 3$. These antibodies mimic natural ligands of the receptor through expression of an RGD integrin-binding motif within CDR-H3 of the antigen recognition site. This feature is combined with specificity for $\alpha v\beta 3$ [17].

Integrin $\alpha v\beta 3$ is expressed by certain invasive tumor types, such as metastatic melanoma, glioma, and breast cancer [7–10, 13]. The receptor is also present on angiogenic blood vessels [3] and serves as an important mediator to secure blood supply for tumor growth. As on metastatic tumor cells, $\alpha v\beta 3$ is activated on angiogenic blood vessels [33] and potentially fulfills similar growth promoting and invasive functions of the sprouting endothelial cells. Integrin $\alpha v\beta 3$ antagonists, targeting the receptor regardless of its functional activation state, have been used in animal models and recently in cancer patients, to curb angiogenesis and slow tumor growth [34]. In the clinic, antibodies against $\alpha v\beta 3$ and a cyclic peptide-based inhibitor of $\alpha v\beta 3$ and $\alpha v\beta 5$ have shown promising effects [14]. MEDI-522, a second generation humanized anti-$\alpha v\beta 3$ mAb showed low toxicity and induced stable disease in some patients with renal metastasis [35].

Generally, integrin ligation supports signal transduction that promotes cell survival, migration and proliferation [36]. Transient expression of the high affinity form of certain integrins in normal cells is tightly regulated and necessary for specific functions. These include leukocyte and platelet interaction with the vessel wall during immune reactions and hemostasis [37]. Expression of activated $\alpha v\beta 3$ and the constitutive presence of the high affinity receptor on disseminating tumor cells may be key for metastatic progression. Thus, therapeutic targeting of the high-affinity conformer of $\alpha v\beta 3$ could offer a focused strategy for interfering with metastatic growth and angiogenic support.

Here, we show that treatment of experimental mice with advanced metastatic disease induced by human tumor cells expressing activated $\alpha v\beta 3$, can stabilize lesion growth and block progression. We applied scFv fragments of patient derived antibodies against the high affinity form of $\alpha v\beta 3$ displayed on phage. This approach increases scFv valency and in vivo half-life. It also takes advantage of the phage tissue penetration properties. In the clinic, this format may not be not preferred but could be replaced with multivalent scFvs, Fab fragments or whole IgG, possibly coupled to toxins or effector molecules [38]. The scFv format could be helpful for diagnosis and tumor cell tracing to report metastatic disease because of the low molecular weight of the scFvs (27 kDa) and their rapid clearance from the circulation and tissues [18, 39]. To gain proof-of-principle information on whether targeting the high affinity conformer of tumor cell integrin $\alpha v\beta 3$ can inhibit advanced and widespread metastatic disease, we increased the challenge for the therapeutic potential of the $\alpha v\beta 3$ directed antibodies and accounted for a spectrum of clinically relevant situations. These included increased tumor burden at the beginning of treatment and the involvement of multiple and differently affected metastatic sites. The observed clinical responses indicated heterogeneity in the metastatic burden in individual animals and different target organs. This situation is clinically relevant and reflects a major challenge for new therapeutic approaches. We demonstrated that scFv antibdody phage can reach metastatic lesions. However, it is possible that not all lesions uniformly absorb the antibody and that some are not efficiently reached by the treatment due, at least in part, to irregularities in the functionality of lesion supporting blood vessels.

Generally, we found that scFv1 is a more potent inhibitor than scFv5. This was seen in the animal studies, particularly under clinically more challenging conditions, but also at the molecular level. Characterizing mechanisms involved in the observed therapeutic response of advanced metastasis to treatment with scFvs against high affinity integrin $\alpha v\beta 3$, we found that the antibodies specifically localize to metastatic lesions and inhibit $\alpha v\beta 3$ ligand binding in the nanomolar range. ScFv 1 is a particularly potent inhibitor and interferes with vitronectin binding 20-fold more effectively, fibronectin binding 17.6-fold more effectively, and fibrinogen binding 30.6-fold more effectively than scFv5.

Both scFvs associate rapidly with $\alpha v\beta 3$ on tumor cells and, in contrast to natural ligand, dissociate extremely slowly. This finding supports the concept that the scFvs may displace natural ligand from the receptor and block the integrin efficiently. This is relevant during adhesion and migration when $\alpha v\beta 3$ temporarily dissociates from its natural ligands. Through this mechanism, the scFvs likely exert long-term inhibitory functions and may effectively impact tumor cell survival and growth mediated by high affinity $\alpha v\beta 3$. In addition to inhibiting activated $\alpha v\beta 3$ on tumor cells, the scFvs might interfere with tumor angiogenesis. We found that the ligand mimetic scFvs react with

the murine receptor. However, we did not see differences in microvessel density in lesions of control versus antibody treated animals.

It is well known that RGD-containing peptides can induce apoptosis by binding to integrins and blocking their functions. Several intriguing reports suggested an additional mechanism through which RGD-containing molecules might impact tumor cell survival [27, 29, 30]. Upon cell internalization, RGD peptides were proposed to interact with an RGD-binding site within procaspase-3 [27, 28]. It was claimed that interactions between the RGD-binding site and RGD-peptides could induce auto-activation of caspase-3. This concept had garnered high attention in the integrin field as it indicated that RGD containing compounds might interfere with tumor cell viability not by inhibiting integrin mediated adhesion, but directly by triggering an apoptotic response through activation of caspase-3, using integrins merely as docking molecules for cell internalization. In fact, we showed earlier that tumor cells expressing activated $\alpha v\beta 3$ can internalize the ligand mimetic scFvs used in this study, and respond with apoptosis [17]. Because of the clinical relevance of our finding that the RGD containing patient derived antibodies could interfere with late stage metastasis, we systematically investigated the ability of the RGD containing scFvs and RGD peptides to bind and directly activate tumor cell caspase-3. However, we did not detect any interaction between caspase-3 and the scFvs or RGD-peptides. In addition, we found no evidence for procaspase-3 activation in cell lysates or using recombinant caspase protein. Therefore, the therapeutic effects of the RGD containing antibody fragments are most likely due to their high affinity to $\alpha v\beta 3$ and potent and persistent ability to interfere with $\alpha v\beta 3$ ligation.

Together, our results indicate that the high affinity conformer of integrin $\alpha v\beta 3$, expressed by a metastatic subset of human tumor cells, is a promising target for inhibition of advanced and widespread metastatic disease. The activated receptor can be efficiently blocked with antibodies from the cancer patient immune repertoire, which interfere with metastatic growth.

Materials and methods

scFv protein and phage production and preparation for in vivo use

ScFv antibodies directed against activated integrin $\alpha v\beta 3$, svFv1 and scFv 5, [17] were displayed as pIII fusion proteins on M13 bacteriophage and expressed in *E. coli*. Phage or scFv protein were purified as described [40]. For in vivo use, endotoxin was removed from phage preparations by repeated phase separations using 1% Triton X-114 [41]. Phage was further purified on protein purification spin columns (Pierce, Rockford IL) and sterile filtered. Phage titer was determined by infecting *E.coli* TG1 with serial dilutions (1×10^4–1×10^{10}-fold) and enumerating colonies on carbenicillin containing agar plates. Phage titers were generally around 10^{11}/ml.

In vivo phage distribution

Phage were injected i.v, i.p or applied intranasally into non-tumor bearing mice to determine phage organ distribution. For intranasal gavage, a phage volume of 10 µl was administered directly into the nostrils in 2 µl increments over 5 min. The organs were harvested and weighed 24 h after phage injection, homogenized in PBS, washed and serially diluted to infect bacteria before counting carbenicillin resistant colonies to calculate the number of phages per gram of tissue.

Analysis of scFv cell binding by flow cytometry

Before use in animals, each scFv phage batch was analyzed by flow cytometry for binding to tumor cells expressing high affinity integrin $\alpha v\beta 3$ in the presence of Ca^{2+} [17]. Phage-ScFvs were used at a concentration of 5×10^8 in TBS and incubated with cells on ice, followed by murine anti-M13 mAb 10 µg/ml (Exalpha Biologicals, Watertown, MA) and goat FITC-anti mouse 1:50 (Zymed, San Francisco, CA).

In vivo treatment of metastatic disease

Advanced metastatic burden for analysis of treatment response was induced by tail vein injection of 6–8 week old CB.17 SCID mice with 1×10^5–2.5×10^5 luciferase tagged MDA-MB 435 or MDA-MB 435-met cells (in vivo selected for enhanced metastatic activity). scFv phage were prepared freshly for each experiment and binding activity validated. Mice were assigned to experimental groups based on non-invasive imaging (photon flux as p/s/cm^2; IVIS 200, Caliper Lifesciences, Alameda, CA) so that control and scFv treatment groups included animals with a similar range of metastatic burden. Under treatment, location and extent of lesion growth were again monitored by bioluminescence imaging, followed by histology.

Deeply anesthetized mice were terminally perfused through the ascending aorta with saline followed by 4% paraformaldehyde (PFA). The perfused organs were post-fixed in para formaldehyde for 4 h before transfer into 25% sucrose in phosphate buffer. Frozen tissues were cryo sectioned (35 µm) and stored in cryoprotective solution at −20°C. For analyses of phage tissue distribution and phage

titer, animals were euthanized 24 h after the last phage injection (i.v., i.p., or intranasal) and organs were weighed and homogenized, followed by infection of bacteria with the extracts. The numbers of carbenicillin resistant colonies (bacteria infected with phage) were counted, and phage count was normalized to phages per gram of tissue. All animal work was performed in accordance with The Scripps Research Institute Animal Resources (AAALAC accredited).

Definition of treatment response and statistical analysis

Late stages of metastatic growth present a high level of complexity and variations in the extent and distribution of metastatic burden from experimental animal to animal. Therefore, we chose analysis criteria similar to "response evaluation criteria in solid tumors" [42–44]. These criteria are used in clinical trials for treatment of advanced metastatic disease to assess individual treatment responses. Treatment responses were evaluated based on longitudinal measurements of tumor cell signal by non-invasive bioluminescence imaging of metastatic burden, before and during treatment in each animal. If, in a given experiment, an animal was treated for 7 days, then lesion growth during the 7-day period before treatment was compared to lesion growth during the 7 days of treatment. The difference in tumor growth before and during treatment was calculated. The resulting fold-changes were defined as: progression (>1.3-fold), stabilization (0.7–1.3-fold), reduced progression (0.1–0.7-fold), or regression (<0.1-fold). It was then determined how the animals in each group distributed between the response categories. For comparison of responses between the three treatment groups, scFv1, scFv5, and wild type phage as control, we note that the overall likelihood ratio chi-squared statistic with six degrees of freedom may be partitioned into two independent components, each with three degrees of freedom: the first component corresponds to comparison of ScFv1 vs. ScFv5, and the second component corresponds to the comparison of controls to the pooled ScFv1/ScFv5 category [45]. We report Fisher exact tests for these component comparisons.

Immunohistochemistry

To detect scFv phage in tumor lesions, free floating tissue sections were quenched with 3% H_2O_2 (in case of DAB staining) and blocked with goat serum for 1 h, before adding a primary antibody against human CD44 (Mab 29.7 at 1:50 dilution of hybridoma supernatant) kindly provided by Jim Quigley, TSRI [21], or M13 phage (anti-M13, Exalpha Biologicals Inc. Watertown, MA, at 20 μg/ml final). After overnight incubation and washing, sections were incubated for 2 h with anti-mouse HRP/Alexa Fluor-594 (4 μg/ml; Invitrogen/Molecular Probes), washed again and placed onto slides for incubation with 3.3-diaminobenzidine as a chromogen for HRP (BD Biosciences). Zink fixed tissues were de-paraffinized and antigen retrieval performed in 1 mM EDTA for 15 min at 100°C followed by treatment as above. Tissues were incubated with primary antibodies anti-mouse F4/80 (5 μg/ml; Cedarlane) or anti-human Ki67 (20 μg/ml; BD Pharmingen) for 1 h, followed by HRP-anti rat (4 μg/ml; Jackson Immunoresearch) or biotinylated anti-mouse(7.5 μg/ml; Vector Laboratories Inc.) antibodies respectively. Following the biotinylation step, tissues were treated with the vectastain ABC kit and all samples were subsequently treated with the peroxidase substrate Vector SG (Vector Laboratories Inc.). Slides were analyzed and images deconvoluted using an AxioImager M1 m microscope and AxioVision 4.6 software (Zeiss, Thornwood, NY). Percent area covered by Ki67 or F4/80 signal relative to lesion area measured was measured with MetaMorph image processing software.

ScFv and ligand binding to purified $\alpha v\beta 3$ receptor protein

Biotinylated natural ligands of $\alpha v\beta 3$: vitronectin (VN), fibronectin (FN) or fibrinogen (Fg) (10 μg/ml) were incubated with purified immobilized $\alpha v\beta 3$ receptor protein in TBS containing Ca^{2+}, Mg^{2+}, and Mn^{2+} (1 mM each), in the presence of increasing concentrations of purified scFv protein. A non-function blocking scFv directed against the integrin αv subunit, scFv 20, was used as a control. Ligand binding was measured after 1 h at 30°C using alkaline phosphatase-conjugated goat-anti-biotin antibody (Sigma at 1:200 dilution of serum), followed by a colorimetric substrate reaction.

Antibody cell binding kinetics

To define conditions for half maximal scFv binding, MDA-MB-435$_{\beta 3D723R}$ cells were incubated with purified FLAG-tagged scFv protein in increasing concentrations of Mn^{2+} (3.75–100 μM). Binding was measured by flow cytometry with murine M2 anti-FLAG antibody (15 μg/ml; Sigma, St. Louis, MO) followed by FITC anti-mouse (30 μg/ml; Pierce). Using the Mn^{2+} concentration (25 μM) that yielded half maximal scFv binding, scFv binding saturation was then measured by incubating MDA-MB-435$_{\beta 3D723R}$ cells for 1 h with increasing concentrations of directly FITC-labeled scFv five protein (2.34–150 μg/ml). The kinetics of scFv cell association and dissociation were analyzed by flow cytometry with directly FITC-labeled scFv protein at half maximal Mn^{2+} concentration and saturating scFv concentration, using MDA-MB-435$_{\beta 3D723R}$

cells. Association time was measured after removing unbound ligand in 10 min intervals. To determine dissociation, cells were first allowed to bind scFv for 1 h to reach binding saturation, after which unbound ligand was removed and the cells washed, before measuring remaining bound scFv in 10 min intervals. FITC-labeled fibrinogen (Fg) was used as a natural ligand for comparison. All incubations were done on ice using ice-cold buffers to prevent scFv or ligand internalization.

Western blot analysis and immunoprecipitation

To study scFv caspase-3 interaction, tumor cells were lysed in RIPA buffer and equal amounts of protein separated, blotted, and detected with rabbit-anti-caspase-3 antibody Sc7148 (0.5 μg/ml; Santa Cruz) followed by goat-anti-rabbit-IgG/HRP conjugate (26.6 ng/ml; Zymed, San Fransisco, CA). Caspase-3 was immunoprecipitated from cell lysates in the presence of protease inhibitors (Roche complete Mini tablet, EDTA-free and 2 mM PMSF) using goat-anti-caspase-3 antibody Sc1225 (1 μg/100 μl lysate; Santa Cruz) and protein G Sepharose beads. Control lysates were incubated with protein G beads only. Precipitated proteins were analyzed on 4–20% SDS–PA gels, blotted and detected with rabbit-anti-caspase-3 (0.5 μg/ml) and goat-anti-rabbit-IgG/HRP conjugate (26.6 ng/ml). Interaction between scFv antibodies and caspase-3 was analyzed by co-immuno precipitation using anti-caspase-3 as above. Flag-tagged scFv 5 (10 μg), or scFv Mut 5 (RGE mutant of scFv 5) as control, were added to cell lysates before western blotting with mouse-anti-Flag (1:500 of Sigma F3165), followed by donkey-anti-mouse-IgG (0.5 μg/ml). Controls included IP without scFv antibodies, addition of scFv 5 but no goat-anti-caspase-3 antibody, and a combination of beads, lysis buffer (instead of lysate) and either scFv 5 or scFv Mut 5.

ELISA-based analysis of caspase-3 and scFv interaction

To analyze binding of caspase-3 to the scFv antibodies, 96-well plates were coated with recombinant procaspase-3 (2 μg/ml) (BioVision, Moutain View, CA), blocked, and incubated with Flag tagged scFv 5 (1–15 μg/ml) or scFv Mut 5 (non RGD containing control) in the presence of 2 mM $MnCl_2$. Binding was measured after incubation with mouse-anti-Flag (Sigma) and donkey-anti-mouse-IgG (Jackson Immuno Research Laboratories, West Grove, PA; all antibodies used at 0.5 μg/ml).

Activation of caspase-3 in hypotonic cell lysates

Activation of caspase-3 in hypotonic lysates of 293A cells or as recombinant protein was measured at end points using the Caspase-Glo 3/7 Assay (Promega) and caspase-3/7 specific peptide sequence Asp-Glu-Val-Asp (DEVD). Hypotonic cell lysates were pepared as desribed [46]. Cell lysates were combined with scFv 5 or scFvMut 5, or with RGD or RAD peptides. Cytochrome *c*/dATP was used as positive control and PBS as negative control. Samples were incubated for 1 h at 37°C, before adding Glo reagent (Promega, Madison, WI) and measuring bioluminescence as relative light units (RUL). GRGDNP was used as RGD peptide and GRADSP as RAD control as reported [27]. Chromogenic substrate reactions were used for continuous measurements of caspase-3 activity. Hypotonic cell lysates were combined with scFv 5 or scFv Mut 5, and DEVD-pNA was added in excess to monitior absorption at 405 nm every 20 s for 2 h at 37°C. Cytochrome *c*/dATP was used as positive control. Maximum reaction velocity (V_{max}) was determined by graphing absorption versus time using the linear graph parts.

Activation of recombinant caspase-3

Recombinant procaspase-3 was expressed in *E. coli* and His-tag purified as described [47]. Recombinant procaspase-3 was incubated with scFv 5, or scFv Mut 5 as control, in caspase assay buffer (50 mM HEPES, pH 7.5, 150 mM NaCl, 0.1% CHAPS, 10% sucrose, 10 mM DTT) in the presence of 1 mM Mg^{2+}. Granzyme B was used as a positive control. Activity was measured based on bioluminescence signal 30 min after adding Glo Reagent. For continuous measurement of recombinant caspase-3 activity, recombinant procaspase-3 was incubated with scFv 5, or scFv Mut 5 as negative control, in PBS with 10 mM DTT, with or without 4 mM $MgCl_2$ for 15 min at 37°C. Ac-DEVD-AFC (100 μM final) was added as fluorgenic caspase-3 substrate and fluorescence measured continuously for 30 min. V_{max} was determined by graphing fluorescence against time.

Acknowledgments We thank Dr. J. Koziol of The Scripps Research Institute for statistical analyses. All animal work was performed in accordance with NIH guidelines and approved by the Institutional Animal Care and Use Committee of The Scripps Research Institute Animal Resources (AAALAC accredited). Grant support: NIH grants CA095458, CA112287 to BFH, CBCRP grants 12NB0176 and 13NB0180 to BFH and DOD grant W81XWH-08-1-0468 to BFH, and fellowships from the Swedish Research Council to KS, and from SG Komen to JSK and ML.

References

1. Steeg PS (2008) Heterogeneity of drug target expression among metastatic lesions: lessons from a breast cancer autopsy program. Clin Cancer Res 14(12):3643–3645
2. Cooper CR, Chay CH, Pienta KJ (2002) The role of $\alpha v\beta 3$ in prostate cancer progression. Neoplasia 4(3):191–194

3. Brooks PC, Montgomery AM, Rosenfeld M et al (1994) Integrin alpha v beta 3 antagonists promote tumor regression by inducing apoptosis of angiogenic blood vessels. Cell 79(7):1157–1164
4. Lim M, Guccione S, Haddix T et al (2005) Avβ3 integrin in central nervous system tumors. Hum Pathol 36(6):665–669
5. Felding-Habermann B, O'Toole TE, Smith JW et al (2001) Integrin activation controls metastasis in human breast cancer. Proc Natl Acad Sci USA 98(4):1853–1858
6. Desgrosellier JS, Barnes LA, Shields DJ et al (2009) An integrin $\alpha v\beta 3$-c-Src oncogenic unit promotes anchorage-independence and tumor progression. Nat Med 15(10):1163–1169
7. Albelda SM, Mette SA, Elder DE et al (1990) Integrin distribution in malignant melanoma: association of the beta 3 subunit with tumor progression. Cancer Res 50(20):6757–6764
8. Gingras MC, Roussel E, Bruner JM, Branch CD, Moser RP (1995) Comparison of cell adhesion molecule expression between glioblastoma multiforme and autologous normal brain tissue. J Neuroimmunol 57(1–2):143–153
9. Gladson CL, Hancock S, Arnold MM, Faye-Petersen OM, Castleberry RP, Kelly DR (1996) Stage-specific expression of integrin $\alpha v\beta 3$ in neuroblastic tumors. Am J Pathol 148(5):1423–1434
10. Ding Q, Stewart J Jr, Olman MA, Klobe MR, Gladson CL (2003) The pattern of enhancement of Src kinase activity on platelet-derived growth factor stimulation of glioblastoma cells is affected by the integrin engaged. J Biol Chem 278(41):39882–39891
11. Brooks PC, Clark RA, Cheresh DA (1994) Requirement of vascular integrin alpha v beta 3 for angiogenesis. Science 264(5158):569–571
12. Fujita Y, Abe R, Shimizu H (2008) Clinical approaches toward tumor angiogenesis: past, present and future. Curr Pharm Des 14(36):3820–3834
13. Cai W, Chen X (2006) Anti-angiogenic cancer therapy based on integrin $\alpha v\beta 3$ antagonism. Anticancer Agents Med Chem 6(5):407–428
14. Desgrosellier JS, Cheresh DA (2010) Integrins in cancer: biological implications and therapeutic opportunities. Nat Rev Cancer 10(1):9–22
15. Paolillo M, Russo MA, Serra M, Colombo L, Schinelli S (2009) Small molecule integrin antagonists in cancer therapy. Mini Rev Med Chem 9(12):1439–1446
16. Schottelius M, Laufer B, Kessler H, Wester HJ (2009) Ligands for mapping $\alpha v\beta 3$-integrin expression in vivo. Acc Chem Res 42(7):969–980
17. Felding-Habermann B, Lerner RA, Lillo A et al (2004) Combinatorial antibody libraries from cancer patients yield ligand-mimetic Arg-Gly-Asp-containing immunoglobulins that inhibit breast cancer metastasis. Proc Natl Acad Sci USA 101(49): 17210–17215
18. Carter PJ (2006) Potent antibody therapeutics by design. Nat Rev Immunol 6(5):343–357
19. Chambers AF (2009) MDA-MB-435 and M14 Cell Lines: identical but not M14 Melanoma? Cancer Res 96(13):5292–5293
20. Hollestelle A, Schutte M (2009) Comment Re: MDA-MB-435 and M14 cell lines: identical but not M14 Melanoma? Cancer Res 69(19):7893
21. Deryugina EI, Quigley JP (2008) Chick embryo chorioallantoic membrane model systems to study and visualize human tumor cell metastasis. Histochem Cell Biol 130(6):1119–1130
22. Byzova TV, Kim W, Midura RJ, Plow EF (2000) Activation of integrin $\alpha v\beta 3$ regulates cell adhesion and migration to bone sialoprotein. Exp Cell Res 254(2):299–308
23. Luo BH, Carman CV, Springer TA (2007) Structural basis of integrin regulation and signaling. Annu Rev Immunol 25:619–647
24. Ajroud K, Sugimori T, Goldmann WH, Fathallah DM, Xiong JP, Arnaout MA (2004) Binding affinity of metal ions to the CD11b a-domain is regulated by integrin activation and ligands. J Biol Chem 279(24):25483–25488
25. Xiong JP, Stehle T, Goodman SL, Arnaout MA (2003) Integrins, cations and ligands: making the connection. J Thromb Haemost 1(7):1642–1654
26. Xiong JP, Stehle T, Goodman SL, Arnaout MA (2003) New insights into the structural basis of integrin activation. Blood 102(4):1155–1159
27. Buckley CD, Pilling D, Henriquez NV et al (1999) RGD peptides induce apoptosis by direct caspase-3 activation [see comments]. Nature 397(6719):534–539
28. Roy S, Bayly CI, Gareau Y et al (2001) Maintenance of caspase-3 proenzyme dormancy by an intrinsic "safety catch" regulatory tripeptide. Proc Natl Acad Sci USA 98(11):6132–6137
29. Anuradha CD, Kanno S, Hirano S (2000) RGD peptide-induced apoptosis in human leukemia HL-60 cells requires caspase-3 activation. Cell Biol Toxicol 16(5):275–283
30. Aguzzi MS, Giampietri C, De Marchis F et al (2004) RGDS peptide induces caspase 8 and caspase 9 activation in human endothelial cells. Blood 103(11):4180–4187
31. Janicke RU, Ng P, Sprengart ML, Porter AG (1998) Caspase-3 is required for alpha-fodrin cleavage but dispensable for cleavage of other death substrates in apoptosis. J Biol Chem 273(25):15540–15545
32. Devarajan E, Sahin AA, Chen JS et al (2002) Down-regulation of caspase 3 in breast cancer: a possible mechanism for chemoresistance. Oncogene 21(57):8843–8851
33. Byzova TV, Rabbani R, D'Souza SE, Plow EF (1998) Role of integrin $\alpha v\beta 3$ in vascular biology. Thromb Haemost 80(5):726–734
34. Stupack DG, Cheresh DA (2004) Integrins and angiogenesis. Curr Top Dev Biol 64:207–238
35. McNeel DG, Eickhoff J, Lee FT et al (2005) Phase I trial of a monoclonal antibody specific for $\alpha v\beta 3$ integrin (MEDI-522) in patients with advanced malignancies, including an assessment of effect on tumor perfusion. Clin Cancer Res 11(21):7851–7860
36. Stupack DG, Cheresh DA (2002) Get a ligand, get a life: integrins, signaling and cell survival. J Cell Sci 115(Pt;%19): 3729–3738
37. Takagi J, Springer TA (2002) Integrin activation and structural rearrangement. Immunol Rev 186:141–163
38. Holliger P, Hudson PJ (2005) Engineered antibody fragments and the rise of single domains. Nat Biotechnol 23(9):1126–1136
39. Colcher D, Pavlinkova G, Beresford G, Booth BJ, Choudhury A, Batra SK (1998) Pharmacokinetics and biodistribution of genetically-engineered antibodies. Q J Nucl Med 42(4):225–241
40. Mao S, Gao C, Lo CH, Wirsching P, Wong CH, Janda KD (1999) Phage-display library selection of high-affinity human single-chain antibodies to tumor-associated carbohydrate antigens sialyl Lewisx and Lewisx. Proc Natl Acad Sci USA 96(12):6953–6958
41. Krag DN, Fuller SP, Oligino L et al (2002) Phage-displayed random peptide libraries in mice: toxicity after serial panning. Cancer Chemother Pharmacol 50(4):325–332
42. Jaffe CC (2006) Measures of response: RECIST, WHO, and new alternatives. J Clin Oncol 24(20):3245–3251
43. Therasse P, Eisenhauer EA, Verweij J (2006) RECIST revisited: a review of validation studies on tumour assessment. Eur J Cancer 42(8):1031–1039
44. Eisenhauer EA, Therasse P, Bogaerts J et al (2009) New response evaluation criteria in solid tumours: revised RECIST guideline (version 1.1). Eur J Cancer 45(2):228–247
45. Agresti A (1990) Categorical data analysis. Sec. 3.3.7. ed
46. Denault JB, Salvesen GS (2003) Expression, purification, and characterization of caspases. Curr Protoc Protein Sci Chap. 21:Unit 21.13.: Unit
47. Stennicke HR, Jurgensmeier JM, Shin H et al (1998) Pro-caspase-3 is a major physiologic target of caspase-8. J Biol Chem 273(42):27084–27090